*metrology*

MDPI

*Article*

# Traceable Metrological Digital Twin for Robot-Based 3D Inspection: Calibration, Uncertainty Propagation, and Cross-Validation

**Brahim Ahmed Chekh [1,*], Asier Garcia Berdote [2], Pablo Puerto [2], Jon Flores [1], Linus Teir [3], Björn Hemming [3] and Naiara Ortega Rodríguez [4]**

[1] TEKNIKER, Calle Iñaki Goenaga, 5, 20600 Eibar, Spain
[2] IDEKO S.Coop. Polígono Industrial, Arriaga Kalea, 20870 Elgoibar, Spain; ppuerto@ideko.es (P.P.)
[3] National Metrology Institute VTT MIKES, Tekniikantie 1, 02150 Espoo, Finland
[4] Department of Mechanical Engineering, Bilbao School of Engineering, Euskal Herriko Unibertsitatea (EHU), Plaza Ingeniero Torres Quevedo, 1, 48013 Bilbao, Spain
* Correspondence: brahim.ahmed@tekniker.es

**Abstract**

Digital Twins (DTs) are increasingly employed in manufacturing to support simulation, monitoring, and control tasks, but their use in dimensional metrology requires explicit traceability and uncertainty information. This work develops a traceable DT for robot-based 3D inspection by integrating an industrial articulated robot with a laser-line triangulation sensor. The methodology combines robot kinematic identification, optical-sensor characterization, sensor-to-robot referencing, and a machine-readable representation of the calibrated metrological state. Uncertainties associated with the calibrated parameters are propagated through the complete measurement chain using a Monte Carlo method aligned with the Guide to the Expression of Uncertainty in Measurement (GUM). Validation combines a CMM-characterized four-sphere artifact and a geo-metrically complex part. For the complex part, two complementary cross-validation routes are considered: dense-surface comparison against a calibrated Triple Scan reference and feature-level comparison against CMM/VCMM reference values and task-specific uncertainties over 67 evaluated characteristics. The results support the use of the DT to generate uncertainty-enriched point clouds while also showing that feature-dependent systematic differences are not fully represented by global point-cloud statistics. The current validation is restricted to the environmental conditions and short-term stability of the experimental campaign; thermal drift and long-term stability are not included in the present model. The proposed framework therefore provides a basis for traceable, uncertainty-aware robot-based inspection and for subsequent industrial qualification under variable operating conditions.

**Keywords:** digital twin; robot metrology; uncertainty propagation; laser triangulation; calibration; hand–eye referencing; Monte Carlo simulation; traceability; optical inspection; industrial inspection robotics

Academic Editor: Patrice Salzenstein

Received: 30 April 2026
Revised: 3 November 2026
Accepted: 5 November 2026
Published: 18 November 2026

**Copyright:** © 2026 by the authors. Licensee MDPI, Basel, Switzerland. This article is an open access article distributed under the terms and conditions of the Creative Commons Attribution (CC BY) license.

## 1. Introduction

With the advancement of digitalization, modeling and simulating real-world processes on a computer has become increasingly significant in the industry. For instance,

simulations are now commonly employed to enhance the understanding of real experiments or to aid in the planning of new experimental setups [1]. In this context, digital twins (DTs) have emerged as pivotal enablers for virtualizing physical systems and their processes in real time. According to ISO 23247-1:2021 [2], a digital twin is defined as a digital representation of an observable manufacturing element, synchronized so that modifications to the physical entity are instantly reflected in the virtual model and vice versa. This standard underscores three key aspects—fidelity, data connectivity, and update rates—that are vital for ensuring that a DT accurately mirrors its real-world counterpart [ISO 23247-1:2021].

However, while ISO 23247 establishes how information should flow between the physical and digital realms, it remains largely agnostic about the quality of that information. Key metrological pillars—traceability, validated uncertainty budgets, and credibility assessment—are either mentioned only in passing or omitted entirely. In practice, this means that two DT implementations that conform to ISO 23247 can deliver radically different levels of accuracy and confidence yet still claim full compliance with the standard.

Most recently, the EU-funded ViDiT project introduced a harmonized framework that unifies these strands.

Our own contribution to that effort—"A Shared Metrological Framework for Trustworthy Virtual Experiments and Digital Twins"—formalized the mathematics of uncertainty propagation across the three DT layers (physical-to-virtual, core model, virtual-to-physical) and illustrated the approach on a CMM and a robot's measurements [3].

Whereas early DT applications focused on fields such as product life-cycle management and predictive maintenance, robotics has recently become one of the most promising domains for implementing digital twins. Industrial robots are increasingly equipped with inspection and measurement functions, which require virtual representations capable of capturing both robot kinematics and sensor behavior. This trend has accelerated the integration of metrological operations directly into robotic manufacturing systems [4].

The widespread adoption of robotic systems across industrial sectors has driven the development of Digital Twins (DT) [5], which are now being applied to industrial robots. These DTs enable the simulation, design, and optimization of robot operations. Several studies have explored different aspects of DT implementation in robotic environments:

- V. Havard et al. [6] proposed a co-simulation and communication architecture between digital twin and virtual reality software, focused on a human–robot collaborative workplace design and assessment.
- N. Kousi et al. [7] presented the use of the digital world modeling of a shop-floor rendered in a 3D environment exploiting the capabilities provided by Robot Operating System RoS, and dynamic update of the DT based on real-time sensor and resource data.
- Y. Cai et al. [8] proposed a methodology using augmented reality to conveniently communicate the layout information between a reconfigurable additive manufacturing system made of robotic arms and its corresponding digital twin for toolpath planning and simulation.

Although the works introduce the use of DT in robotic environments, these are not mainly focused on the modeling of the robot but rather on the working environment and the process, where the robot modeling is carried out using commercial software, for example, RoS. Only a limited number of studies have directly addressed the development of digital models specifically focused on the robot itself. As an example, M. Matulis and C. Harvey [9] developed a Digital Twin of a robotic arm and trained it using artificial intelligence techniques. Their virtual environment was implemented in Unity, where a virtual robotic arm was linked to its corresponding physical system.

https://doi.org/10.3390/metrology6040088

In parallel, several studies have investigated the performance of laser triangulation sensors under different measurement conditions [10]. However, these studies are generally focused on specific sensor-performance tests and do not necessarily address the complete measurement chain encountered in robot-based inspection of complex geometries. In such applications, the final measurement result depends not only on the optical sensor performance, but also on the positioning of the sensor relative to the measured surface.

For example, Mohammadikaji et al. [11] investigated uncertainty propagation in 3D shape measurement using laser triangulation while explicitly considering positioning errors. Their work highlights the importance of including positioning-related contributions in the uncertainty model. In the present study, this aspect is further addressed by experimentally characterizing the robot-positioning contribution and incorporating it, together with the optical-sensor contribution, into the uncertainty model of the complete robot-based inspection system.

In response to the limitations observed in current digital twin implementations—particularly the absence of integrated metrological criteria—this study proposes a Digital Twin architecture for a robotic 3D inspection system that combines an articulated-arm robot with a laser line triangulation sensor. The specific contribution of the present work lies at the system-integration level, through the integration of a metrological framework that ensures traceability, credibility, and uncertainty quantification throughout the measurement process. This includes the characterization of uncertainty sources originating both from the sensor and from the robot's positioning system, as well as the implementation of a traceable calibration and referencing procedure. The proposed DT enables the propagation of these uncertainties through the virtual model, supporting virtual measurement evaluations with quantified reliability. In doing so, the system moves beyond conventional DT applications and contributes to the foundation of a metrologically credible digital inspection infrastructure for robotic systems in industrial environments.

A study of the variables in the physical world has been conducted in order to introduce the errors into the virtual world. Relevant uncertainty sources in the physical system were characterized and transferred to the virtual model, where they were propagated using Monte Carlo simulations. [12]. In some studies, temperature has been excluded due to its minimal contribution to the overall uncertainty [13]

Previous studies have therefore addressed several of the individual elements required for metrologically reliable robotic inspection. Digital Twins have been developed for robotic operation and positioning, while other works have focused on uncertainty evaluation for optical and laser-line scanning systems. In particular, Digital Twins of optical measurement systems have demonstrated the possibility of determining task-specific measurement uncertainty and evaluating alternative scanning strategies. Similarly, uncertainty propagation models for laser triangulation have considered the influence of positioning errors, while recent metrological DT approaches for industrial robots have introduced traceable calibration and uncertainty evaluation of robot positioning. These contributions provide important foundations for the present work; however, they address different parts of the complete robot-based optical measurement chain. Mohammadikaji et al. [11] investigated uncertainty propagation in laser-triangulation-based 3D measurement, explicitly considering the influence of positioning errors on the reconstructed geometry. Zhao et al. [13] focused on the uncertainty associated with the dimensional calibration of a line-laser scanning measurement system. In a different context, Ostrowska et al. [14] discussed the implementation and assumptions of Digital Twins in coordinate metrology. Although these studies provide relevant foundations for uncertainty-aware and digitally supported measurement systems, they address specific elements of the overall inspection process rather than the complete uncertainty propagation through an integrated industrial robot–sensor measurement chain.

https://doi.org/10.3390/metrology6040088

To clarify the positioning of the present work with respect to the existing literature, Table 1 summarizes the main characteristics addressed by representative studies, including robot modeling, optical measurement, metrological calibration and traceability, uncertainty evaluation, and the integration of the robot–sensor measurement chain within a Digital Twin framework.

**Table 1.** Comparison of representative Digital Twin and uncertainty-aware approaches for robotic and optical measurement systems. Note: ✓ indicates that the corresponding characteristic is explicitly addressed in the cited study; "–" indicates that it is not addressed or not reported. Additional text within the cells specifies the particular implementation or scope considered in each study.

| Study | Robot/ Positioning Model | Optical 3D Measurement | Metrological Calibration/ Traceability | Uncertainty Evaluation | Integrated Robot–Sensor Inspection DT |
|---|---|---|---|---|---|
| Havard et al. [6] | ✓ | – | – | – | – |
| Kousi et al. [7] | ✓ | Sensor data | – | – | – |
| Matulis and Harvey. [9] | ✓ | – | – | – | – |
| Mohammadi-kaji et al. [11] | Positioning error | ✓ Laser triangulation | – | ✓ | – |
| Vlaeyen et al. [15] | CMM positioning | ✓ Laser line scanner | ✓ | ✓ | Optical DT, CMM-based |
| Sepahi-Boroujeni and Khameneifar [16] | – | ✓ 3D scanning | ✓ | ✓ | Scanner-focused |
| Maculotti et al. [3] | ✓ Industrial robot | – | ✓ | ✓ | Robot-positioning DT |
| Present work | ✓ Calibrated robot model | ✓ Laser line scanner | ✓ Robot + sensor + hand–eye referencing | ✓ At point-cloud level | ✓ |

Accordingly, the contribution of the present work does not rely on introducing a new robot calibration algorithm, sensor characterization method, hand–eye calibration technique, or Monte Carlo formulation individually. Instead, the work focuses on their integration within an operational metrological Digital Twin for in-process robotic 3D inspection. The proposed framework connects the physical calibration of the robot, the metrological characterization of the laser-line sensor, and the sensor-to-robot referencing procedure with their corresponding virtual models. Calibrated parameters and their associated uncertainty information are maintained as part of the DT state and subsequently used during virtual measurements to transfer the metrological information through the complete measurement chain to the resulting scanned point cloud.

In this context, the specific contribution of the proposed DT is threefold. First, it establishes a traceability chain linking reference measurements, robot and sensor calibration, and the parameterization of the virtual measurement system. Second, it provides a structured and interoperable representation of the calibrated DT state, including model parameters, uncertainty information, and calibration metadata. Third, it applies this metrologically enriched model to the integrated robot–sensor system and evaluates its

behavior against physical measurements on both a calibrated artifact and a geometrically complex part. The resulting approach operationalizes the metrological framework previously proposed in [3] for a robot-based optical inspection application.

To facilitate a clear understanding of the methodology and contributions presented, the remainder of this article is structured as follows:

Section 2 details the materials and methods, beginning with an overview of the robotic system and optical sensor, followed by their respective modeling, calibration, and characterization procedures. It then introduces the Digital Twin implementation, including its traceability structure, uncertainty modeling approach, and virtual environment setup. Section 3 presents experimental results, covering robot and sensor calibration, as well as integrated system validation within the DT framework. Section 4 discusses the implications of these findings in the broader context of industrial metrology and digital twin development. Finally, Section 5 provides the conclusions and outlines future directions for extending the framework to additional robotic platforms and inspection strategies.

## 2. Materials and Methods

### *2.1. Materials*

The Digital Twin (DT) system presented in this study consists of a robotic arm equipped with an integrated optical sensor, designed to detect deviations in manufactured parts. This integrated metrological setup is developed on a machining robot, combining robotic flexibility with high-precision optical sensing for robot-based inspection, with in-process inspection as the intended application. Its objective is to assess part geometry during manufacturing and support quality assurance by identifying dimensional deviations during inspection. The complete measurement chain is shown in Figure 1.

The DT is structured by addressing each subsystem of the measurement process:

- The robot system.
- The optical measurement sensor.

The referencing and calibration procedure for the sensor and robot.

The coordinate systems and transformations used throughout the DT are also summarized in Figure 1. In the notation adopted in this work, $SC_{Base}$, $SC_{Flange}$, $SC_{Scanner}$, and $SC_{Obj}$ denote the robot-base, robot-flange/TCP, optical-sensor, and measured-object coordinate systems, respectively. $SC_{WO}$ denotes the work-object coordinate system used for robot programming and measurement referencing. A homogeneous transformation $T_B^A$ represents the rigid-body transformation that expresses coordinates defined in frame $B$ with respect to frame $A$. The complete transformation chain therefore connects a point measured in the scanner coordinate system with the robot base and, subsequently, with the workpiece reference system.

The following subsections describe in depth the materials used to develop the Digital Twin of the 3D scanning robotic system. First, the robotic system is introduced, highlighting its configuration, control architecture, and suitability for precision positioning tasks.

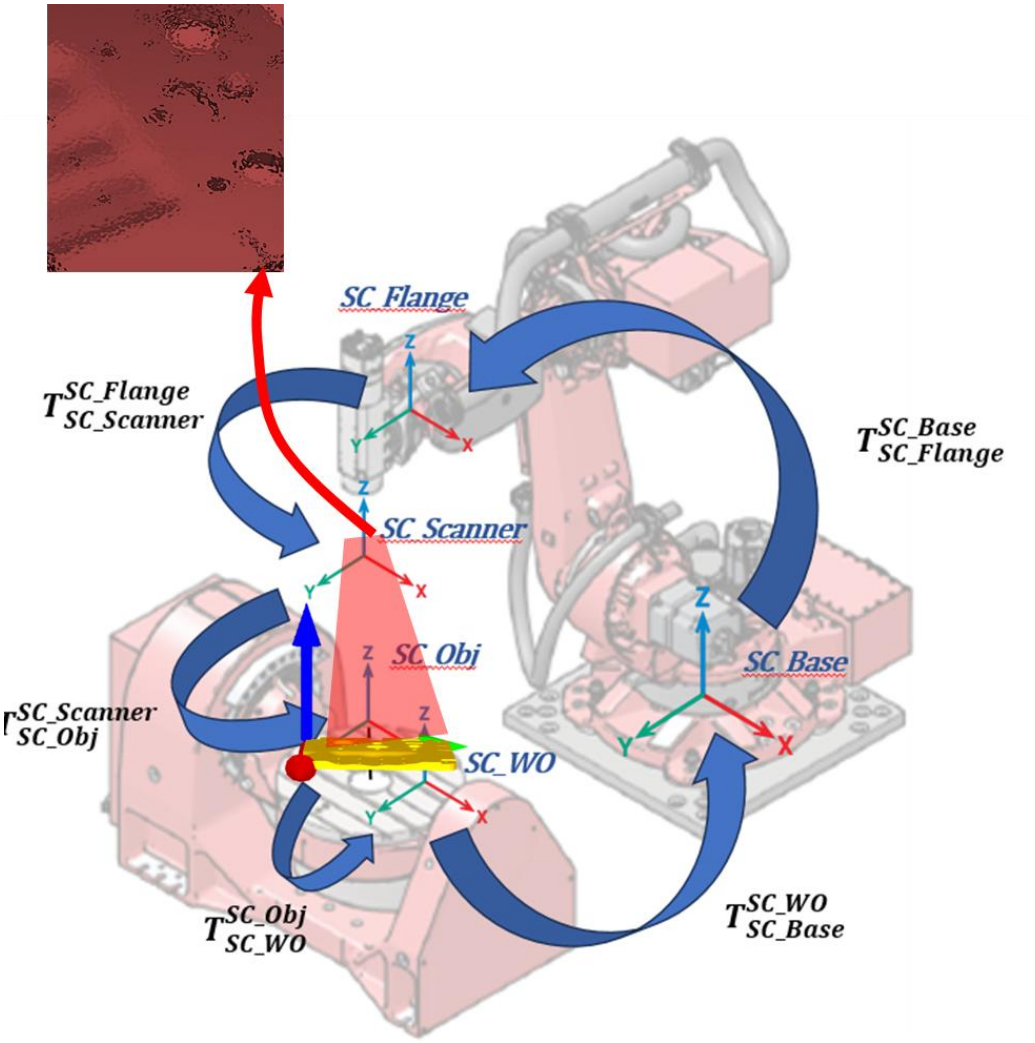
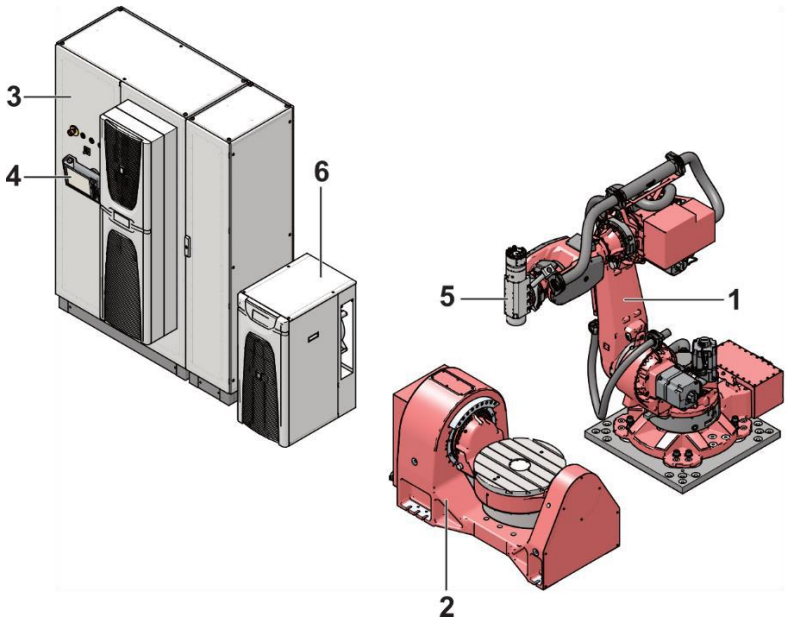



**Figure 1.** Overview of the Digital Twin and the coordinate-transformation chain of the robot–sensor measurement system.

#### 2.1.1. Robot System

The robotic manipulator used is a MABI MAX-100-2.25-P (MABI Robotic AG, Veltheim, Switzerland) six-axis industrial robot (see Figure 2). This model has an approximate reach of 2.25 m and a maximum payload of 100 kg, making it suitable for carrying the 3D sensor around large structures like a train chassis. The robot is equipped with high-resolution encoders on each joint and is controlled by a Siemens Sinumerik (840D) CNC controller (Siemens AG, Erlangen, Germany), ensuring precise and smooth motion trajectories. With repeatability on the order of 20 µm, the robot meets the performance thresholds typically required for metrological applications, allowing it to be reliably used in high-accuracy dimensional inspection tasks.




| | | | |
|---|---|---|---|
| **1** | ROBOT MAX-100-2.25-P | **2** | ROTARY TILT TABLE MMT-500-DE |
| **3** | CONTROL CABINET MRC | **4** | HT 10 TEACH PENDANT |
| **5** | END-EFFECTOR/TOOL MOUNTING INTERFACE | **6** | COOLING UNIT |

**Figure 2.** Robot system overview.

#### 2.1.2. The Optical Measurement System

The optical measurement component (Figure 3) integrated in the robotic system is the LMI Gocator 2430A-3R-B-01-S (LMI Technologies Inc., Burnaby, BC, Canada), a laser line triangulation sensor designed for high-resolution 3D surface inspection. This sensor projects a laser line onto the target surface and captures its deformation using a built-in camera to generate a dense profile of height points. By synchronizing these profiles with the robot's motion, a full 3D point cloud of the scanned surface can be reconstructed.

The Gocator 2430 sensor operates at a wavelength of 660 nm and delivers a field of view ranging from 25 mm to 80 mm, depending on the standoff distance. It provides a vertical resolution of up to 1.2 µm and lateral resolution below 40 µm, which makes it well suited for capturing small surface details and deviations. The sensor operates at frame rates up to 5 kHz, allowing fast and dense data acquisition during continuous robot motion. The high-speed 3D data output is streamed via Gigabit Ethernet and synchronized through encoder inputs to match robot trajectory execution.

In this setup, the sensor is mounted rigidly on the flange of the robot arm. Its orientation is configured to maintain the laser plane orthogonal to the surface during scanning, maximizing triangulation accuracy. The system also includes tools for laser alignment, calibration block referencing, and height validation, all of which are described in subsequent sections.

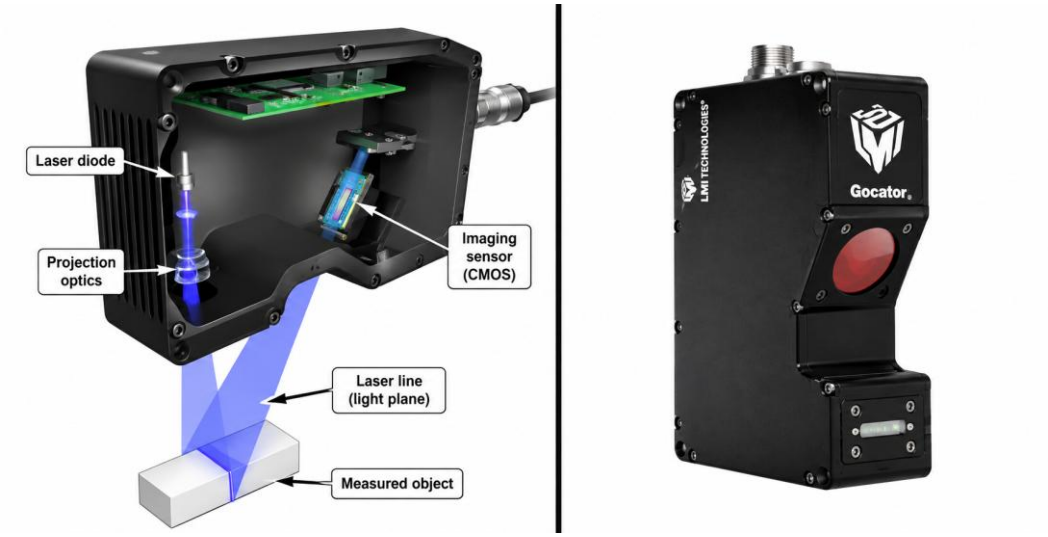



**Figure 3.** The optical measurement system used in this study: (**left**) schematic representation of the laser-line triangulation principle; (**right**) LMI Gocator 2430A-3R-B-01-S optical 3D sensor.

### *2.2. Methods*

To guide the reader through the construction of this system, this section is structured as follows:

- First, the conceptual design of the Digital Twin is presented, including the architecture and the metrological framework that governs its operation. This encompasses the identification of uncertainty sources, their modeling, and the propagation mechanisms implemented to simulate their influence throughout the measurement chain.
- Second, the modeling and characterization of the robotic system is detailed. This includes the derivation of the nominal kinematic structure and the integration of joint compliance parameters.
- Third, the optical measurement sensor is introduced and characterized. The procedures for alignment, height measurement, and repeatability evaluation using certified ceramic gauge blocks are explained.
- Finally, the sensor-to-robot referencing method is described, and the implementation of the complete Digital Twin system is outlined.

#### 2.2.1. Digital Twin Implementation

The implementation of the Digital Twin (DT) aims to ensure the metrological traceability of the robot-based measurement system by maintaining a synchronized, uncertainty-aware virtual replica of the physical inspection setup. The DT reflects not only the kinematics of the robot and the sensor, but also the behavior of the measurement system under calibrated and updated conditions, thereby enabling reliable virtual measurements and informed decision-making during in-process inspection.

The implementation is structured as illustrated in Figure 4 The diagram is structured into two main blocks that represent the two complementary loops in which the Digital Twin (DT) operates: the Calibration Cycle (top half) and the Measurement Cycle (bottom half). Each cycle bridges the virtual and real domains, illustrating how the DT interacts dynamically with physical systems to ensure traceable and uncertainty-aware measurements.

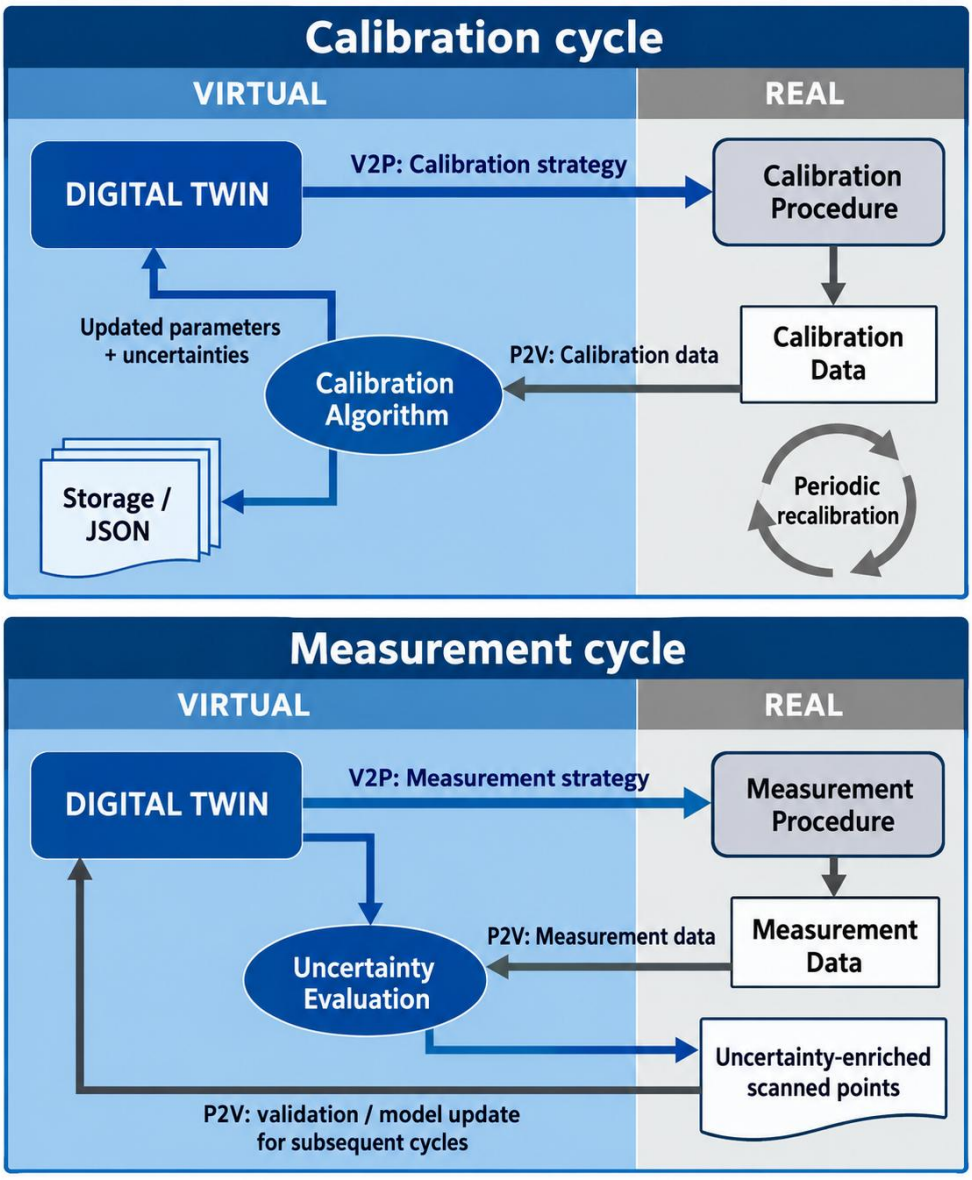



**Figure 4.** Bi-directional P2V/V2P workflow of the metrological Digital Twin. The upper panel represents the calibration cycle, in which physical calibration data update the DT parameters and associated uncertainties. The lower panel represents the measurement cycle, in which the calibrated DT defines the measurement strategy and evaluates the uncertainty associated with the acquired scanned points.

Calibration Block (P2V–Physical to Virtual)

During the calibration cycle, physical calibration and referencing procedures provide the experimental data required to update the virtual model. Calibration residuals, transformation parameters, and the corresponding uncertainty information are processed by the calibration algorithms and incorporated into the DT. The resulting calibrated parameters, uncertainties, and traceability metadata are stored in the machine-readable data structure and subsequently used during measurement planning. Calibration is therefore treated as a recurrent Physical-to-Virtual update rather than as a one-time initialization.

Measurement Block (V2P–Virtual to Physical)

During the measurement cycle, the calibrated DT is used to evaluate measurement strategies and to propagate the uncertainty associated with the robot, optical sensor, and sensor-to-robot referencing chain. The selected measurement strategy is transferred to the

physical system for execution, while the acquired point-cloud data are returned to the virtual environment for uncertainty evaluation. The resulting output consists of scanned points associated with point-wise uncertainty estimates, which can be used for subsequent validation and planning cycles.

Data Structure and Interoperability

The machine-readable representation of the Digital Twin is organized as a hierarchical metrological data model (JSON-based files). Rather than reproducing the internal software implementation directly, the data structure is organized according to the physical and metrological functions of the measurement system. The principal information blocks, summarized in Figure 5, comprise system identification and conventions, the nominal robot model, calibrated robot parameters, dynamic and load information, referencing parameters, calibration records, parameter uncertainties, and the optical sensor model.




**Figure 5.** Hierarchical organization of the machine-readable metrological Digital Twin data model.

The DT data structure is organized into separate blocks representing the nominal robot model, calibrated parameters, dynamic and load information, referencing data, calibration records, uncertainty information, and the optical sensor model. The system-identification block defines the conventions required for an unambiguous interpretation of the model, including units, kinematic conventions, joint limits, and reference configurations. The nominal and calibrated robot models are stored independently, allowing successive calibration states to be incorporated without modifying the original robot definition.

Dynamic and load-related quantities, such as gravity, link masses, centers of gravity, and tool properties, are retained to support the representation of load-dependent deformations.

The referencing block contains transformations linking the optical sensor, robot, and workpiece coordinate systems, together with information on the reference artifact and the associated referencing uncertainty. Calibration metadata, including the procedure, reference instrument, measured poses, identified parameters, and residual statistics, are stored together with the calibrated model. Standard uncertainties associated with the identified robot and referencing parameters provide the statistical inputs for the Monte Carlo propagation. Finally, the optical-sensor block contains the characterization results, including alignment parameters, the position-dependent systematic-error map, and the corresponding repeatability map, which are propagated together with the robot and referencing contributions to the resulting point cloud.

Figure 6 shows a simplified excerpt of the JSON structure used to represent the metrological state of the Digital Twin. The robot model, calibration results, referencing information, parameter uncertainties, and optical sensor characterization are integrated within the same hierarchical machine-readable structure. The nominal and calibrated robot parameters are maintained separately, while the referencing block defines the transformation between the optical sensor and the robot coordinate system. The optical sensor block incorporates the characterization results, including alignment parameters, systematic-error correction, and position-dependent measurement variability. This organization allows the complete metrological state of the robot–sensor system to be reconstructed and used directly as input to the uncertainty-propagation model.

To provide a concise overview of the machine-readable DT structure, Table 2 summarizes the main information blocks contained in the JSON data model and their role within the metrological Digital Twin. The table highlights the relationship between the nominal and calibrated robot model, the referencing information, the calibration history, the associated parameter uncertainties, and the optical sensor characterization data. This structure allows the DT to retain not only the numerical model parameters, but also the metrological information required to reconstruct the calibrated state of the robot–sensor measurement system and to support subsequent uncertainty propagation.

**Table 2.** Main information blocks of the machine-readable metrological Digital Twin data model.

| Information Block | Main Content | Function Within the DT |
|---|---|---|
| **System identification and conventions** | Robot identification, units, kinematic and rotation conventions, joint limits and repeatability | Ensures unambiguous interpretation of model parameters |
| **Nominal robot model** | Nominal DH parameters, robot base, flange, stiffness and compliance | Defines the initial geometric and elastic robot model |
| **Dynamic and load parameters** | Gravity, link masses and centers of gravity, tool mass and CoG | Supports calculation of load-dependent robot deformation |
| **Calibrated robot model** | Identified DH, base, flange and stiffness/compliance parameters | Represents the current calibrated state of the robot |
| **Referencing parameters** | Sensor-to-robot transformation, workpiece/reference frame, reference artifact and referencing uncertainty | Establishes the geometrical link between sensor, robot and measured object |
| **Calibration information** | Calibration date, procedure, commanded configurations, external measurements and calibration errors | Links calibrated parameters to the physical calibration process |

| | | |
|---|---|---|
| **Parameter uncertainty model** | Standard uncertainties associated with robot and referencing parameters | Defines input distributions for Monte Carlo uncertainty propagation |
| **Optical sensor model** | Sensor characterization, alignment, systematic-error map and repeatability map | Represents the calibrated metrological behavior of the optical sensor |

```
{
  "systemIdentification": {
    "robot": "Robot_ID",
    "kinematicConvention": "Modified I
    "lengthUnit": "mm",
    "angleUnit": "deg"
  },

  "nominalRobotModel": {
    "DHParameters": {
      "a": [...],
      "alpha": [...],
      "d": [...],
      "theta": [...]
    },
    "base": {...},
    "flange": {...},
    "jointCompliance": [...]
  },

  "calibratedRobotModel": {
    "DHParameters": {...},
    "base": {...},
    "flange": {...},
    "jointCompliance": [...]
  },

  "referencingParameters": {
    "sensorToRobotTransformation": {
      "translation": [...],
      "rotation": [...]
    },
    "workpieceReference": {...},
    "referencingUncertainty": {...}
  },

  "parameterUncertainties": {
    "robotKinematics": {...},
    "robotCompliance": {...},
    "referencing": {...}
  },

  "opticalSensorModel": {
    "alignment": {
      "pitch": "...",
      "roll": "..."
    },
    "characterization": {
      "systematicErrorMap": [...],
      "standardDeviationMap": [...]
    }
  }
}
```

**Figure 6.** Simplified example of the JSON-based implementation of the metrological Digital Twin data structure.

Uncertainty Assignment from Calibrated DT Parameters

In the presented system, the calibrated parameters of the robotic model—joint offsets, stiffness values, sensor-to-tool transformations—are periodically estimated via structured procedures and stored in machine-readable JSON structures. These files not only contain nominal parameter values but also include metadata such as estimated standard deviations, covariance structures, and validation residuals, forming a complete metrological profile of the system.

A critical element of the Digital Twin (DT) framework is the assignment and propagation of measurement uncertainty from the physical calibration stage to the virtual measurement result. In the proposed implementation, the uncertainty model is structured according to the main elements of the robot–sensor measurement chain (Table 3). Four groups of input quantities are considered: robot-related parameters, optical sensor parameters, sensor-to-robot referencing parameters, and calibration/reference-related quantities. This decomposition preserves the physical origin of the uncertainty contributions and provides the input uncertainty budget subsequently propagated through DT.

Temperature and other environmental quantities were not independently recorded as input quantities during the present experimental campaign and are therefore not included in the current uncertainty model. No thermal-error compensation or experimentally validated thermo-geometric model is claimed in this work. Consequently, the calibrated DT state and the reported uncertainty results are considered valid for the environmental conditions prevailing during the calibration, referencing, and measurement campaign. Application under varying shop-floor thermal conditions would require explicit environmental sensing and an experimentally identified thermal model of the robot–sensor measurement chain.

**Table 3.** Main uncertainty sources considered in the Digital Twin measurement model.

| Uncertainty Group | Main Input Quantities | Source of Uncertainty Information | Representation in the DT |
|---|---|---|---|
| Robot model | Calibrated kinematic parameters; joint compliance parameters | Robot calibration | Calibrated value and associated standard uncertainty |
| Optical sensor | Position-dependent systematic deviation; measurement dispersion | Gauge-block characterization | Systematic correction map and local standard deviation |
| Sensor-to-robot referencing | Parameters of the sensor-to-tool transformation | Hand–eye calibration | Calibrated transformation parameters and associated uncertainties |
| Calibration/reference quantities | Reference artifact and calibration-related quantities | Traceable calibration/reference data | Reference values and associated standard uncertainties |

The robot-related contribution includes the parameters identified during robot calibration, including the calibrated kinematic parameters and the parameters describing joint compliance. The optical sensor contribution is obtained from the experimental characterization described in Section 2.2.2 and includes the position-dependent systematic deviation and the dispersion observed in repeated measurements. The sensor-to-robot referencing contribution is associated with the parameters defining the transformation between the sensor coordinate system and the robot tool frame obtained during the hand–eye calibration procedure. Finally, the calibration/reference contribution accounts for the uncertainty associated with the reference quantities used during the calibration and

referencing stages. Table 3 summarizes the uncertainty sources considered in the DT and their corresponding origin.

The assignment of probability distributions to these quantities follows the metrological framework described by Maculotti et al. [3], in which the estimates of the model parameters and their associated uncertainty information constitute the input to the uncertainty propagation through the virtual model. In the present implementation, the uncertain calibrated parameters are represented using Gaussian probability distributions. For an input parameter $\hat{q}_i$, the corresponding random quantity is defined as

$$Qi \sim N(q\hat{}\, i\,, u2(qi)) \tag{1}$$

where $\hat{q}_i$ is the value estimated from the corresponding calibration or characterization procedure and $u(q_i)$ is its associated standard uncertainty. Therefore, the meaning of each distribution is given by the calibrated parameter value, while its standard deviation corresponds to the associated $1\sigma$ uncertainty obtained from the same calibration process. In this way, the probability distributions used by the DT are directly linked to the experimentally determined metrological state of the physical system rather than being assigned from generic nominal specifications.

For the optical sensor, the experimentally determined systematic-error map is used to correct the measured value according to its location within the sensor measurement range, while the dispersion obtained from the repeated measurements defines the random contribution. After systematic correction, this contribution is represented by a zero-mean Gaussian distribution whose standard deviation depends on the measurement position:

$$E_{sensor}\,(X,Z) \sim N(0,\sigma^2\,(X,Z)) \tag{2}$$

where $\sigma^2\,(X,Z)$ is derived from the characterization measurements and interpolated over the sensor measurement range.

The uncertainty propagation is subsequently performed using a Monte Carlo method in accordance with the GUM Supplement 1 approach. For each simulation, realizations of the uncertain input quantities are generated from their assigned Gaussian distributions and introduced into the complete robot–sensor measurement model. The resulting set of simulated coordinates provides an empirical probability distribution for each point of the scanned point cloud. From this distribution, the expected coordinate values, associated standard uncertainties, and coverage intervals can be evaluated.

The uncertainty propagation is applied to the complete robot–sensor measurement model. For a point measured in the sensor coordinate system, its coordinates in the workpiece reference frame are obtained as

$$\tilde{p}_W = (T_W^B)^{-1} T_F^B(q,\theta,\kappa) T_S^F(\eta) \tilde{p}_{S,\mathrm{corr}}, \tag{3}$$

where $B$, $F$, $S$, and $W$ denote the robot base, flange/tool, sensor, and workpiece frames, respectively. The vectors $\theta$, $\kappa$, and $\eta$ contain the calibrated kinematic, elastic, and sensor-to-robot referencing parameters, while $\tilde{p}_{S,\mathrm{corr}}$ includes the systematic correction obtained from the sensor characterization.

Due to the nonlinear nature of the complete robot–sensor transformation chain, the uncertainty evaluation is performed numerically using Monte Carlo propagation. Considering the uncertain model inputs in the vector $x$, the measurement model can be written as $y = f(x)$ for each Monte Carlo realization $m$, an input vector $x^{(m)}$ is generated from the assigned probability distributions and propagated through the complete measurement model according to

$$y^{(m)} = f\left(x^{(m)}\right) \tag{4}$$

The resulting ensemble of output coordinates is subsequently used to estimate the statistical properties and coverage intervals associated with each reconstructed point.

A convergence study was performed to determine the number of Monte Carlo realizations required for stable uncertainty estimation (Figure 7). The number of simulation realizations was progressively increased while monitoring the resulting uncertainty estimates. The results showed that the uncertainty values became substantially stable after approximately 20,000 realizations. At 40,000 realizations, the difference in the estimated uncertainty between successive evaluated realization counts was below 0.01 mm. Therefore, 40,000 Monte Carlo realizations were adopted for the uncertainty evaluations reported in this study.

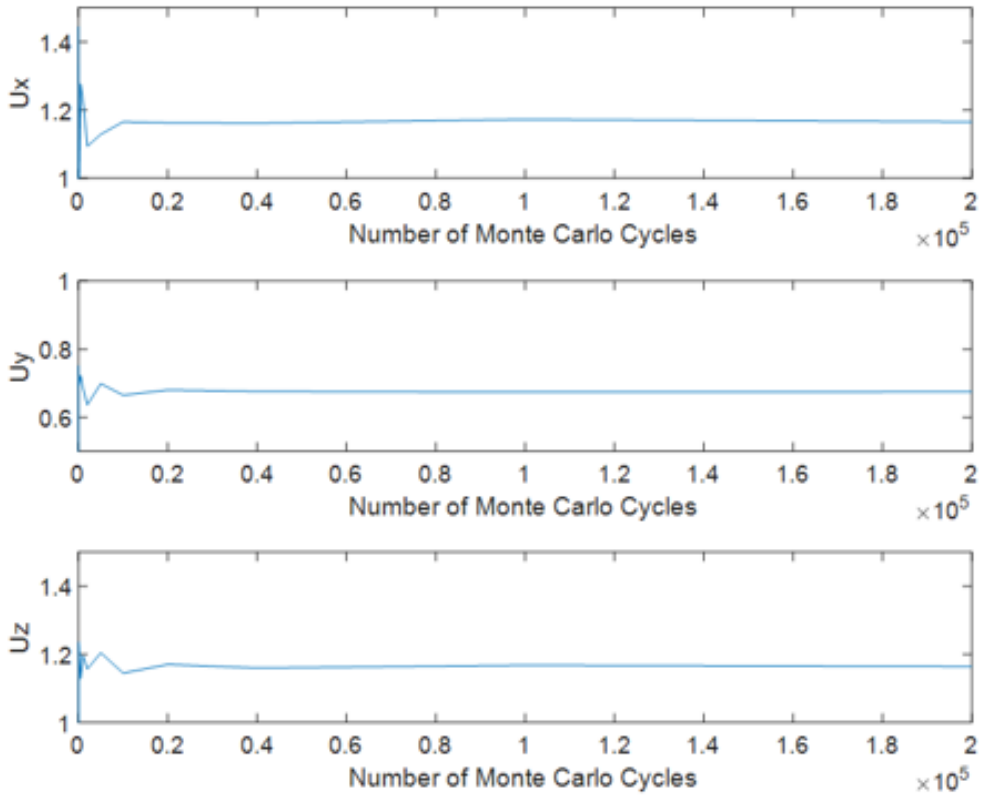



**Figure 7.** Convergence of the estimated Cartesian-coordinate uncertainties as a function of the number of Monte Carlo realizations. The stabilization of the uncertainty estimates is used to select the number of realizations adopted for the subsequent uncertainty-propagation analyses.

The computational cost increased approximately linearly with the number of realizations, with an average processing time of approximately 0.0173 s per Monte Carlo realization. The selected number of realizations therefore represents a compromise between numerical convergence and computational cost. This computational demand also motivates the future implementation of surrogate models for uncertainty-aware applications requiring shorter evaluation times.

This implementation follows the Physical-to-Virtual (P2V), core-model, and Virtual-to-Physical (V2P) uncertainty propagation principles described in the shared metrological framework presented in [3]. Calibration and characterization provide the parameter estimates and their associated uncertainty information in the physical-to-virtual stage; these quantities are propagated through the DT measurement model; and the resulting uncertainty is finally associated with the virtual measurement output at point-cloud level.

Virtual Environment and Digital Twin Operation

The functional implementation of the Digital Twin in this work relies on a dual-software environment combining RoboDK (v5.9) and MATLAB (v2024b). Figure 8 presents representative screenshots of both environments during the implementation of the robotic inspection workflow. RoboDK provides the virtual robot-cell interface for visualization, offline programming, and communication with the robot controller, whereas MATLAB serves as the computational environment for kinematic modeling, calibration, uncertainty propagation, and measurement-data processing.

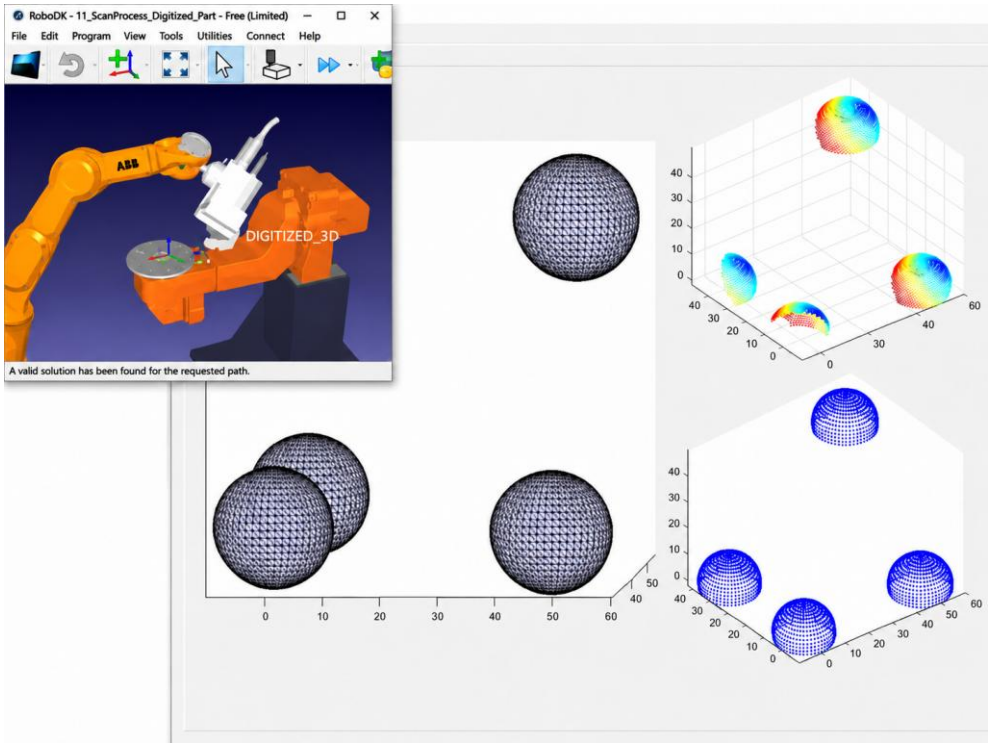



**Figure 8.** Software environments used in the Digital Twin implementation: RoboDK for robot-cell visualization and offline programming, and MATLAB for calibration, data processing, and analysis.

MATLAB serves as the computational core of the Digital Twin, implementing the robot kinematic model, calibration routines, Monte Carlo uncertainty propagation, and uncertainty-aware measurement planning. It is also used for sensitivity analysis and processing of calibration and measurement data required for model validation.

RoboDK provides the virtual robot-cell environment used for 3D visualization, offline programming, virtual commissioning, and communication with the physical robot controller. It supports the execution of measurement paths defined from the strategies evaluated in MATLAB.

The integration of MATLAB and RoboDK therefore provides a bidirectional implementation in which calibration and measurement data are used to update the DT, while the virtual model supports the definition and execution of measurement strategies. This combination links the metrological computation with the operational robot environment throughout the inspection workflow.

This layered implementation ensures that each stage of the DT operation—from calibration to inspection—remains both metrologically valid and computationally tractable, paving the way for scalable, traceable inspection in flexible robotic systems.

2.2.2. Robot Modeling and Calibration

The modeling of the robotic system is a critical component in the development of the Digital Twin (DT), enabling high-fidelity simulation of the robot's behavior during scanning tasks. The robot's virtual model is constructed using the modified Denavit–Hartenberg (DH) convention, which provides a systematic representation of each joint and link via four geometric parameters (see Figure 9). These parameters define the transformation matrices between successive coordinate frames, allowing for accurate computation of the end-effector pose from joint angles.

In addition to geometric parameters, the robot model incorporates joint stiffness parameters to account for elastic deformations under load. These compliance effects become relevant when high accelerations or payloads are present, as they introduce small but significant deviations in the end-effector position. Inspired by the methodology presented in [17], the joint elasticity is modeled as a linear relation between applied torque and angular deflection, with each joint characterized by an individual stiffness coefficient. These parameters are particularly important for applications requiring sub-millimetric accuracy, such as robotic metrology.

Additionally, the model includes definitions of both the robot base frame and the tool center point (TCP), which are crucial for accurate transformation between the robot's coordinate system and the part reference frame.

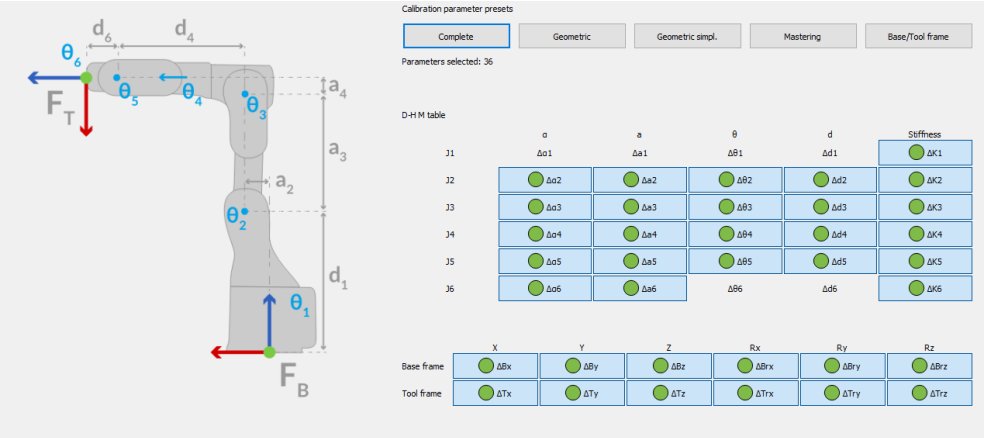



**Figure 9.** Parametric robot model implemented in RoboDK, including the modified Denavit–Hartenberg kinematic parameters, joint stiffness parameters, and robot base and tool-frame definitions.

Joint elasticity is represented using a first-order compliance model (Equation (5)). For joint j, the load-induced angular deflection is defined as

$$\Delta qj = \frac{kj}{\tau j} \quad (5)$$

where $\tau j$ is the applied joint torque and $kj$ is the corresponding joint-stiffness coefficient. The corrected joint coordinate is then introduced into the forward-kinematic model.

The objective of this formulation is to represent the first-order influence of load-dependent joint deformation on the robot pose. It is not intended to reproduce the complete structural behavior of the manipulator; no dedicated load-deflection experiment was performed to independently validate each coefficient.

The combination of geometric and elastic modeling allows the DT to simulate the robot's pose under realistic operating conditions, considering both rigid-body transformations and load-induced deviations. This model not only improves the predictability of

scanning trajectories but also enables the evaluation of deformation-induced uncertainty, which is propagated through the DT to the final point cloud analysis.

To ensure high geometric fidelity and traceability between the physical system and its digital twin, an external measurement-assisted calibration procedure was implemented [17]. Robot calibration aims to identify deviations in both geometric and referencing parameters with respect to the nominal model. For this purpose, an AT901-MR laser tracker was used to measure a sequence of robot poses defined specifically for calibration. The robot was programmed to reach multiple configurations with varied orientations and positions, increasing the excitation of geometric errors in the kinematic chain. This strategy was applied by using a multi-target approach—incorporating three reflector spheres instead of one—attached to a custom tool at the robot end-effector. This modification enables the identification of parameters that are otherwise non-observable, particularly those associated with the wrist joints.

To ensure the accuracy and reliability of the robotic system for dimensional metrology tasks, a full-pose calibration procedure was implemented, targeting all six degrees of freedom (DoF) of the robot's kinematic structure. The goal of this calibration is to identify and compensate for systematic deviations between the nominal robot model and its real geometric behavior. The approach follows a model-based parameter identification strategy, wherein a set of measured poses from an external reference system is compared against the robot's internal kinematic estimates.

The calibration process is based on collecting pose data from 16 distinct robot configurations. For each pose $i$, the end-effector position and orientation are simultaneously recorded from two sources:

The robot's internal parameter-based forward kinematics $\mathbf{T}_{\text{robot}}^{(i)}$,

An external metrological reference system providing ground-truth measurements $\mathbf{T}_{\text{ref}}^{(i)}$.

These transformation matrices $\mathbf{T} \in SE(3)$ represent the homogeneous transformation from the robot base to the tool center point (TCP). The objective is to find a set of correction parameters $\boldsymbol{\theta}$, which include robot parametrization, that minimizes the discrepancy between the measured and estimated poses.

The optimization problem is formulated as a nonlinear least squares minimization (see Equation (6)):

$$\min_{\boldsymbol{\theta}} \sum_{i=1}^{N} \| \mathbf{T}_{\text{ref}}^{(i)} - \mathbf{T}_{\text{robot}}^{(i)}(\boldsymbol{\theta}) \|_F^2 \tag{6}$$

where

$N = 16$ are the number of calibration poses.

$\|\cdot\|_F$ denotes the Frobenius norm, used to quantify the deviation between transformation matrices.

$\mathbf{T}_{\text{ref}}^{(i)}$ is the measured pose using an external metrological reference.

$\mathbf{T}_{\text{robot}}^{(i)}(\boldsymbol{\theta})$ is the estimated pose using the current kinematic parameters.

The calibration parameters are collected in the correction vector $\boldsymbol{\theta}$, which represents the deviations of the selected robot-model parameters from their nominal values. Accordingly, the calibrated parameter vector is expressed as

$$\mathbf{p}_{cal} = \mathbf{p}_{nom} + \boldsymbol{\theta} \tag{7}$$

where $\mathbf{p}_{nom}$ contains the nominal robot-model parameters and $\boldsymbol{\theta}$ contains the corrections identified during calibration. Depending on the selected identification model, $\boldsymbol{\theta}$ includes corrections to the modified Denavit–Hartenberg parameters (link lengths, link offsets, twist angles, and joint zero offsets), together with the additional base, flange/tool, and compliance-related parameters included in the calibration.

The optimal correction vector $\boldsymbol{\theta}$ is obtained by minimizing the discrepancy between the poses measured by the external metrological reference and those predicted by the calibrated forward-kinematic model.

This procedure enables the fine-tuning of the robot model so that the Digital Twin can replicate the real motion behavior with high accuracy, thereby ensuring consistency and traceability in the 3D inspection results. The final calibrated parameters are integrated into the DT structure for subsequent uncertainty propagation and path planning processes.

#### 2.2.3. Optical Measurement Implementation and Characterization

The first step in the methodology was to align the laser profilometer with the plane of the multi-axis platform, where the ceramic blocks were placed. This alignment was performed by adjusting two angular parameters: pitch and roll of the laser profiler (see Figure 10).

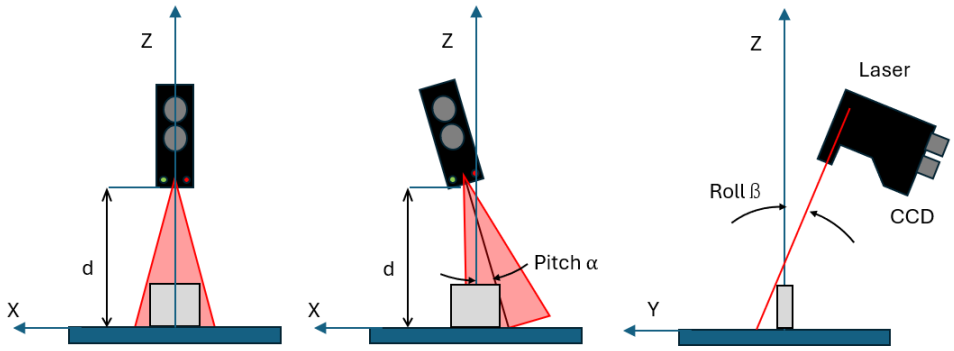


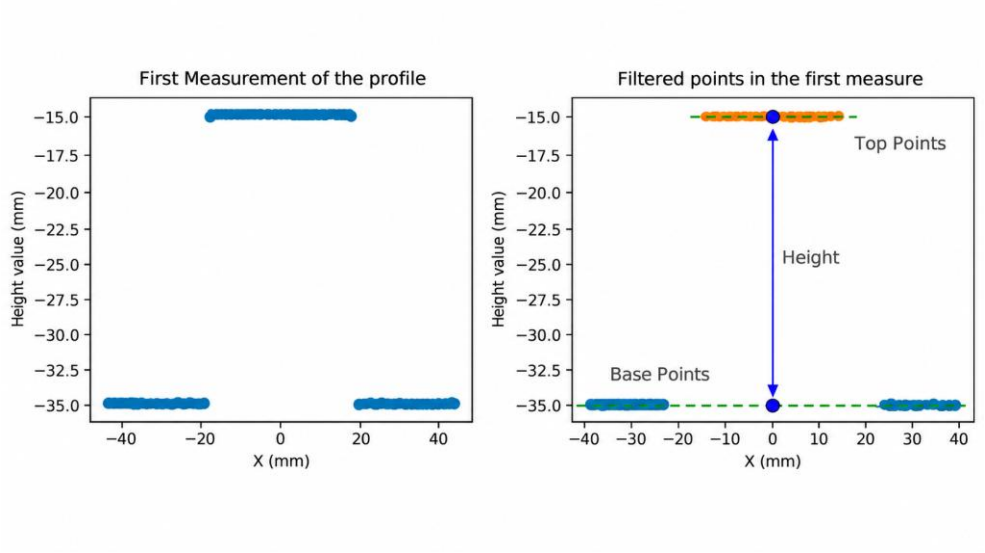

**Figure 10.** Example of height calculation, starting from the raw measured line (**left**) and ending with filtered and separated points (**right**).

- The pitch angle (rotation about the *Y*-axis, which is perpendicular to the laser plane) influences how the laser perceives the empty platform. Ideally, a perfectly aligned laser should register the platform as a straight horizontal line. In this step, the pitch was manually adjusted to make the measured line as horizontal as possible.
- The roll angle was calibrated using a 5 mm ceramic block. A series of measurements were taken for different roll angles, and the selected angle was the one yielding the lowest measured height. This criterion ensures that the laser plane is as perpendicular as possible to the platform plane, achieving an incidence angle of the laser on the surface near to 90º.

Before proceeding with the laser alignment and sensor characterization, it is essential to define the method used to compute the measured height of the ceramic blocks from the acquired laser profiles (see Figure 11). The process consists of the following steps:

1. A ceramic block is measured, and the points are first classified into two groups—"floor surface" and "block surface"—through a threshold value. Then, 10% of points at the borders are removed to avoid artifacts generated by the edges of the block.
2. A linear fit is applied separately to each group, and outliers are removed using the interquartile range (IQR) method. Specifically, only data points within the range [Q1 − 1.5 × IQR, Q3 + 1.5 × IQR] are retained, where Q1 and Q3 are the first and third quartiles, respectively.
3. For each surface, the Z-coordinate is interpolated at a reference X-value located in the middle of the data range.

4. The height of the block is then computed as the difference between the interpolated Z-values of the block and floor surfaces.




(**a**) (**b**)

**Figure 11.** Example of height calculation, starting from the raw measured line (**a**) and ending with filtered and separate points (**b**).

This method ensures a reliable and consistent height measurement while minimizing the influence of noise and outliers in the laser data.

Once the laser alignment was completed, the actual characterization process was performed. The following procedure was repeated for different gauge blocks of heights 5, 10, 20, 30, 40, 50, 60, and 70 mm:

1. The gauge block was placed in three different positions on the platform (left, center, and right), as illustrated in Figure 12.
2. At each position, 1000 measurements were acquired, with the process being fully automated, so it takes approximately 5 min. The repeated acquisitions performed during this characterization are used to quantify the short-term repeatability of the optical sensor under fixed measurement conditions. The standard deviation obtained for each height and lateral position is therefore interpreted as a repeatability contribution and subsequently incorporated into the sensor uncertainty model. These measurements should not be interpreted as a complete Gauge Repeatability and Reproducibility (GR&R) study, since the characterization was performed using a fixed experimental configuration and does not include operator-to-operator variability or independent re-establishment of the measurement setup.
3. For each measurement, the block height was computed using the previously described height calculation method. The mean height was then obtained from the 1000 measurements at each position. This step required minimal computational resources, with an average processing time of approximately 1 min.
4. Finally, the Nominal-Measured deviations were analyzed for all cases to evaluate the accuracy and precision of the system. Accuracy was calculated, given one position, as the distance from each data point to the fitted to straight line and the points for that position.

Based on the characterization values, it is necessary to determine the systematic error and its standard deviation. A map covering the entire measurement range of the sensor has been obtained by using calibration blocks of different heights, positioned at the left, center, and right of the sensor. To estimate the error at any measurement point, a linear

extrapolation approach has been adopted. This adjustment enables fast and efficient calculation for any given XZ coordinate

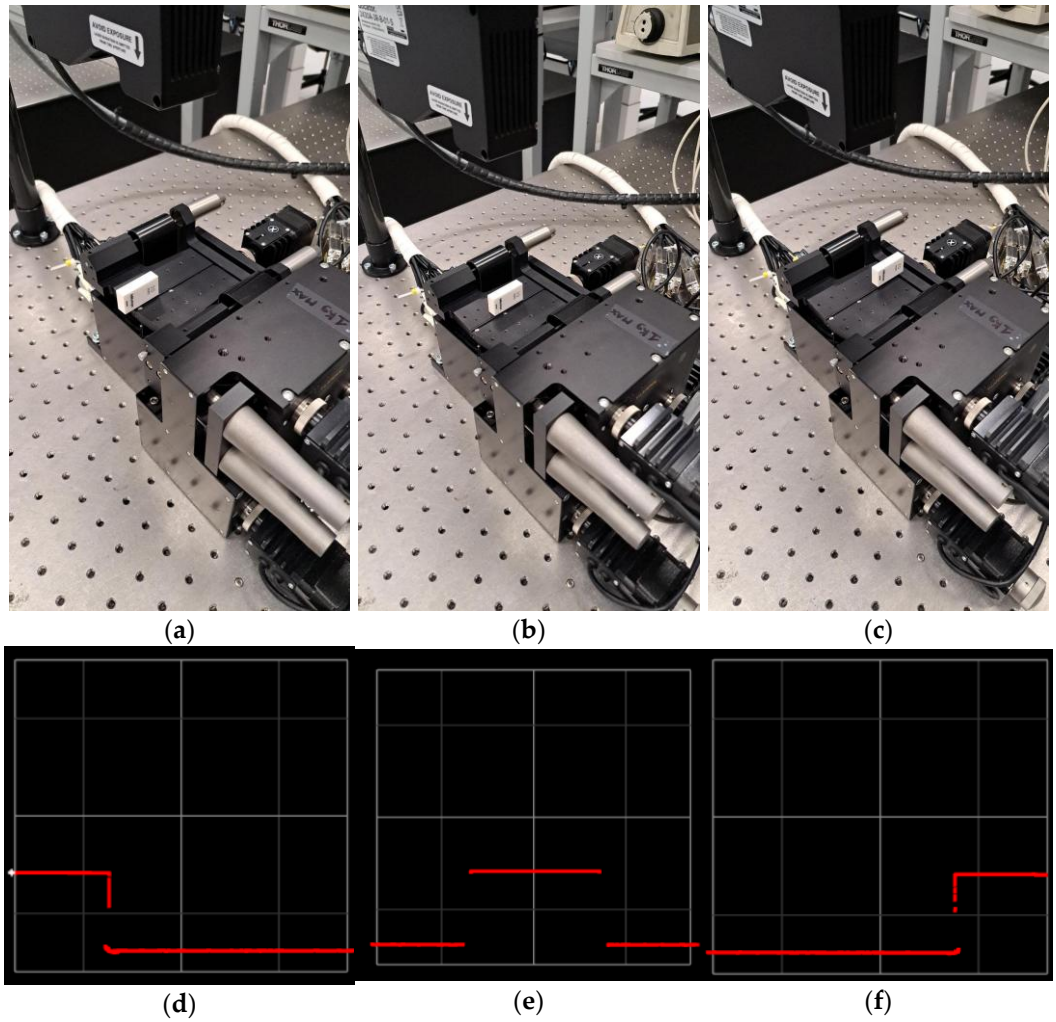



**Figure 12.** Location of one block gauge (white part) in the three positions where the sensor is tested. Physical set-up: (**a**) left, (**b**) center and (**c**) right, and the corresponding signals (**d**), (**e**) and (**f**).

The characterization data obtained at different depths and lateral positions are used to construct a position-dependent systematic-error map $b(X, Z)$. The measured sensor coordinate is corrected according to

$$Zcorr = Zmeas - b(X, Z) \quad (8)$$

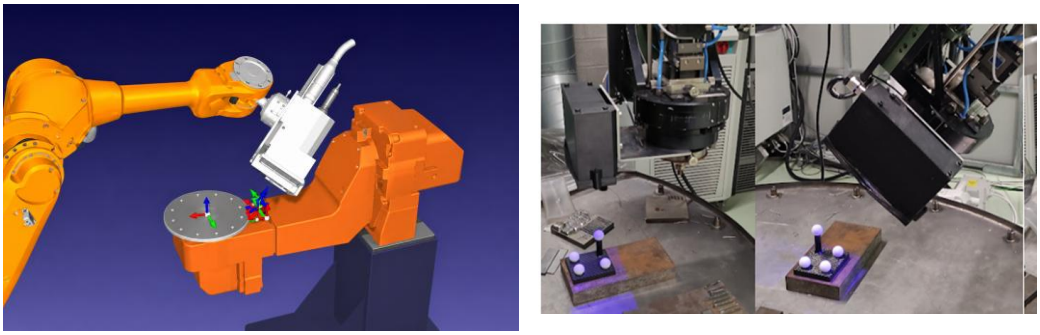
where $b(X, Z)$ is obtained by interpolation of the experimentally measured deviations. After this correction, the remaining sensor contribution is represented by the local repeatability standard deviation $\sigma(X, Z)$, which is subsequently propagated through the Digital Twin uncertainty model.

### *2.3. Sensor-to-Robot Referencing*

For the referencing of the laser sensor, a fully integrated and automated procedure was designed (see Figure 13). The process is based on scanning a specially designed artifact composed of 4 balls, which had been previously characterized using a coordinate measuring machine (CMM). The known positions of the spheres, combined with the laser-scanned point clouds, allow for a best-fit alignment between the sensor frame and the robot's tool frame. The referencing routine is executed in a multi-orientation mode to ensure robustness and minimize sensitivity to scanning direction or occlusions.

The four-sphere artifact, previously characterized by CMM, is scanned from multiple robot configurations and orientations. The resulting transformation is evaluated by transforming the measured sphere centers into a common reference system and comparing them with the CMM-characterized geometry.

The sensor-to-robot referencing is formulated as a conventional hand–eye calibration problem. This method corresponds to a hand–eye calibration procedure, in which the transformation between the sensor coordinate system and the robot's tool center point (TCP) is computed by observing a known calibration object from various robot poses. As described in Garmendia et al. (2020) [18], the approach uses a four-sphere reference pattern fabricated using additive manufacturing and characterized through FDM scanning and sphere fitting. By applying the Tsai–Lenz algorithm to solve the transformation chain, the relative pose of the sensor with respect to the robot's TCP is derived. This makes it possible to accurately map the scanned point cloud from the sensor's frame to the robot base frame, ensuring geometric consistency for further operations. The process is validated by repeating the scan from different poses and confirming the alignment of the calculated coordinate systems. This calibration step is crucial to enable reliable referencing and subsequent quality control operations based on the 3D scanning data.



(**a**) (**b**)

**Figure 13.** Sensor-to-robot referencing procedure using the four-sphere artifact: (**a**) virtual representation of the robot–sensor configuration in RoboDK; (**b**) physical acquisition of the calibrated artifact from different robot orientations.

This procedure ensures the spatial referencing of the optical sensor with respect to the robot while preserving the traceability information associated with the reference artifact and the calibration procedure. The uncertainty associated with the reference artifact is subsequently propagated through the kinematic-identification and sensor-to-robot referencing stages into the Digital Twin. The uncertainty of the reference artifact is propagated through the kinematic identification and referencing stages into the DT. As a result, the subsequent point-cloud measurements can be associated with uncertainty estimates derived from the calibrated robot–sensor measurement chain, a fundamental requirement for achieving reliable in-process inspection in smart manufacturing contexts.

## 3. Results

This section outlines the key results obtained from the development and application of the Digital Twin (DT) for the robotic 3D inspection system.

The experimental assessment followed a hierarchical validation strategy, progressing from subsystem characterization to evaluation of the complete robot–sensor measurement chain. At the subsystem level, the optical sensor was characterized using calibrated ceramic gauge blocks covering nominal heights from 5 mm to 70 mm. Measurements were performed at three lateral positions within the sensor measurement range, with 1000

repeated acquisitions for each condition. These experiments provided systematic-error and repeatability information subsequently incorporated into the Digital Twin uncertainty model. Robot performance was independently evaluated through the kinematic calibration and residual analysis described in Section 3.1.

Following these individual evaluations, the complete robot–sensor system was assessed using two complementary experimental parts in Section 3.2. The objective of this stage was not to perform an exhaustive acceptance test covering all possible geometric measurands, but to evaluate the behavior of the integrated metrological DT after robot calibration, sensor characterization, and sensor-to-robot referencing.

### *3.1. Robot Calibration*

The calibration results presented here are a direct outcome of the kinematic calibration procedure described previously in the Methods Section 2.2.2. As detailed there, the robot calibration process consists of identifying optimal values for the parameters of the robot model by minimizing the difference between the robot's estimated pose and that measured by an external reference system. This is formulated as a nonlinear least-squares problem, where the objective function is the residual pose error, and the optimization iteratively adjusts the model parameters until the improvement between iterations becomes negligible.

To evaluate the performance of the calibrated model, 16 diverse robot poses were used, each capturing different configurations across the robot's workspace. For each pose, the residual position and orientation errors were computed by comparing the robot's internal estimate with the corresponding measurement from the external system.

As shown in the results:

The position residuals (Figure 14) exhibit an average Euclidean error norm of 0.031 mm, with a standard deviation of 0.014 mm and a maximum observed error of 0.064 mm. The component-wise residuals remain symmetrically distributed with standard deviations under 0.023 mm, highlighting the consistency of the positional calibration across all axes.

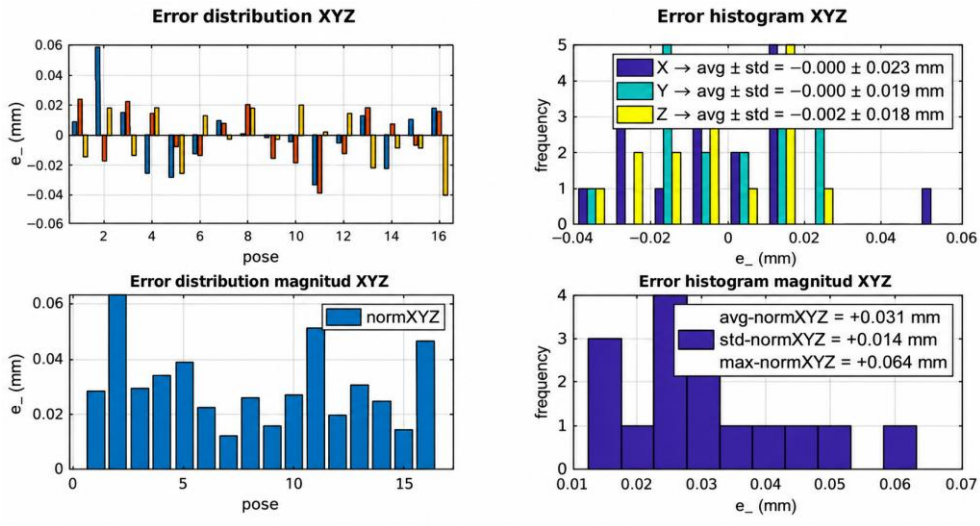



**Figure 14.** Position residuals of the calibrated robot evaluated over the 16 validation poses, showing the component-wise position errors together with the distribution and histogram of the Euclidean position-error norm.

The orientation residuals (Figure 15) yield an average rotational norm error of 0.022 degrees, standard deviation of 0.010 degrees, and maximum deviation of 0.050 degrees.

Individual axis errors (Rx, Ry, Rz) similarly remain centered around zero with low dispersion.

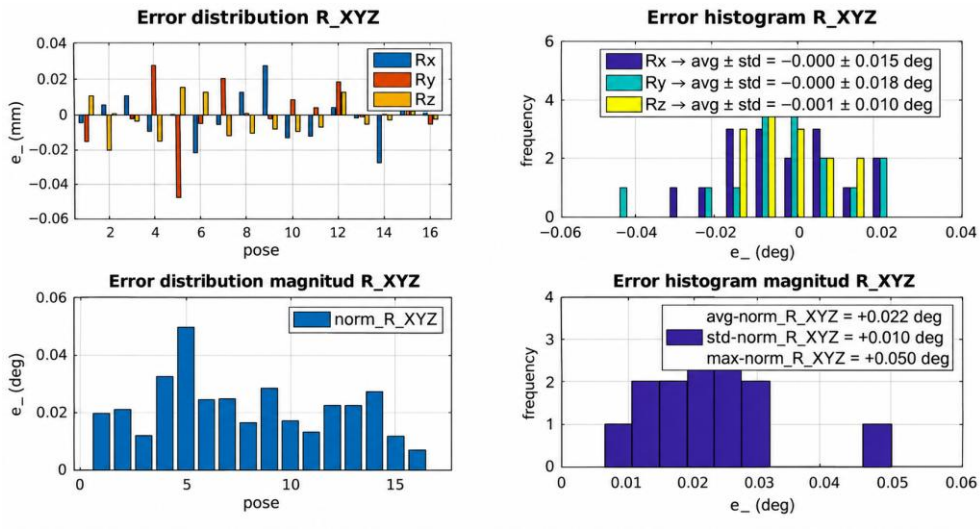



**Figure 15.** Robot orientation error after calibration and orientation residuals after robot calibration: component-wise rotational errors and distribution of the rotational-error norm over the 16 evaluated poses.

These metrics demonstrate that the calibration procedure effectively enhances the fidelity of the robot's forward kinematics, thereby increasing the reliability of its positioning for precision inspection tasks. The low spread and magnitude of the residuals confirm the system's suitability for use in metrologically traceable robotic measurement environments. The following section further elaborates on the identified kinematic parameters and their associated uncertainties.

Additionally, and following the robot calibration process, a set of kinematic parameters—mainly Denavit–Hartenberg (DH) parameters—were identified. These include the link lengths (a), twist angles ($\alpha$), link offsets (d), and joint angles ($\theta$). Although the model includes additional parameters such as joint stiffness to account for elastic deformation, these results focus on the DH parameters for clarity and illustration.

The table below (Table 4) summarizes the estimated values of the DH parameters for each joint, along with their corresponding standard uncertainties. These uncertainties were computed as part of the identification process, in accordance with the Guide to the Expression of Uncertainty in Measurement (GUM) and are crucial for subsequent uncertainty propagation in the digital twin.

**Table 4.** Identified Denavit–Hartenberg (DH) parameters and their associated standard uncertainties after robot calibration.

| Joint | a [mm] ± u(a) | $\alpha$ [°] ± u($\alpha$) | d [mm] ± u(d) | $\theta$ [°] ± u($\theta$) |
|---|---|---|---|---|
| 1 | 0.000 ± 0.000 | 0.000 ± 0.000 | 0.000 ± 0.000 | 0.000 ± 0.000 |
| 2 | 339.230 ± 0.410 | −90.029 ± 0.013 | 0.000 ± 0.000 | −89.833 ± 0.021 |
| 3 | 999.624 ± 0.681 | 0.023 ± 0.037 | −1.942 ± 0.329 | −0.066 ± 0.011 |
| 4 | 172.650 ± 0.405 | −89.928 ± 0.021 | 904.323 ± 0.564 | −0.005 ± 0.003 |
| 5 | 0.706 ± 0.143 | 89.972 ± 0.013 | 0.190 ± 0.053 | 0.011 ± 0.006 |
| 6 | −0.620 ± 0.132 | −90.016 ± 0.010 | 0.000 ± 0.000 | 180.000 ± 0.000 |

### *3.2. Sensor*

The resulting deviations between the nominal values and experimental measurements of the gauge-block heights are plotted below (Figure 16). It can be observed that the left side follows a different trend, which could be caused by the deviation observed in Figure 17. The left position exhibits a different trend, which is further discussed below.

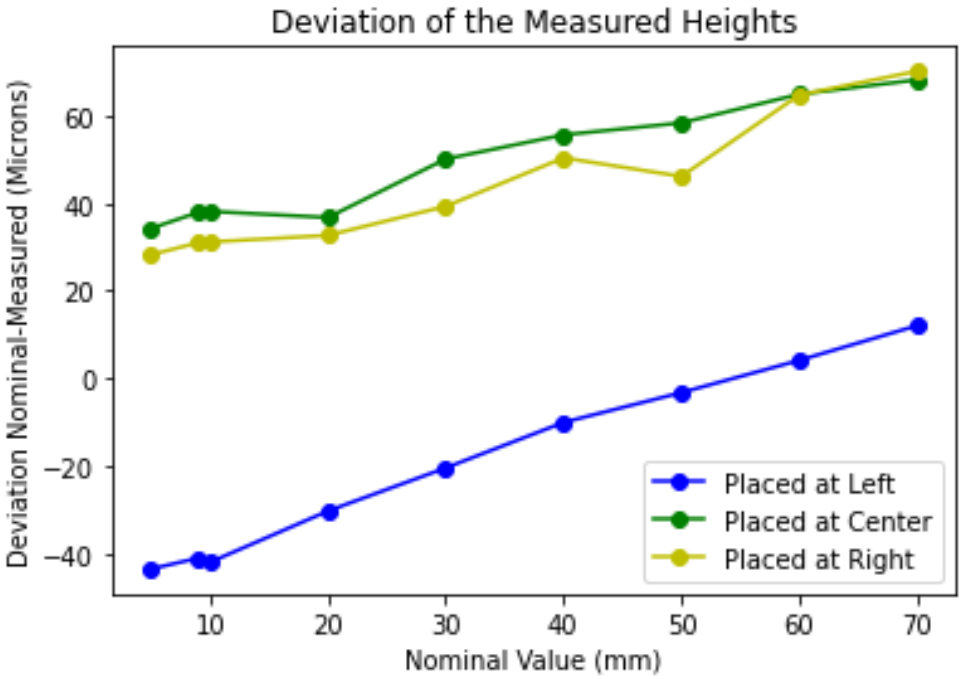



**Figure 16.** Deviation in microns of each ceramic gauge, distinguished in Left, Center and Right positions.

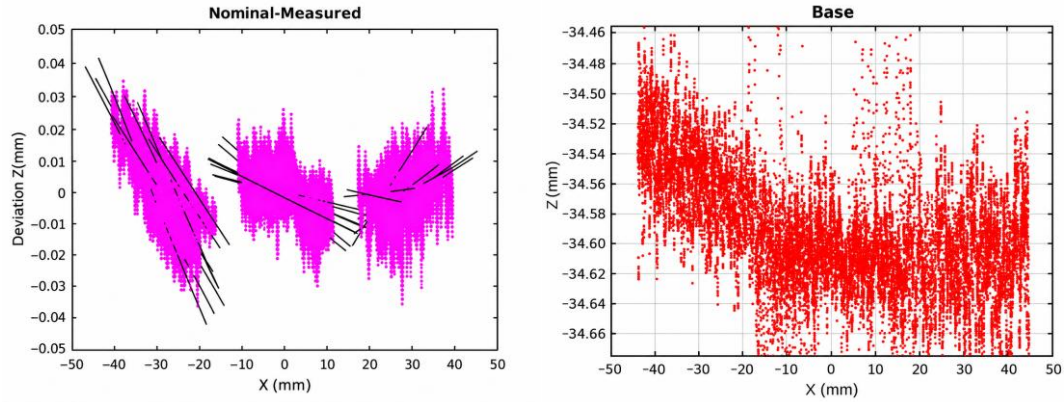
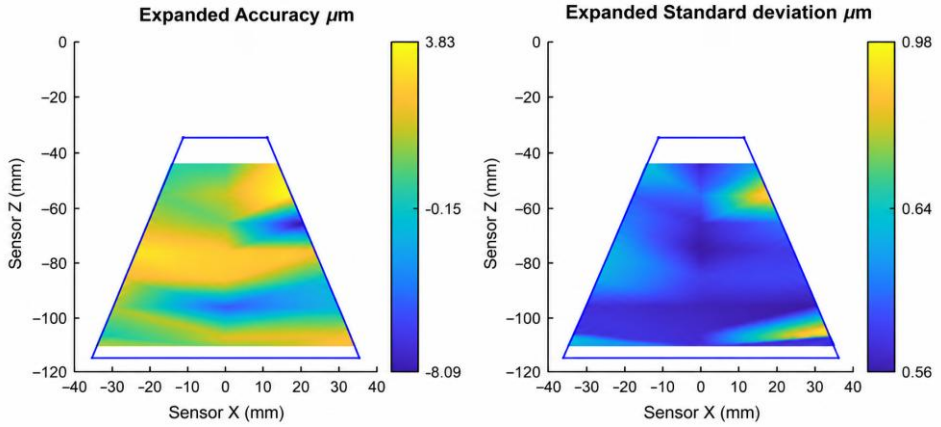



**Figure 17.** Representation of all deviations (**left**) and laser measurements on the empty platform (**right**), showing a problem with the left position.

Accuracy and standard deviations for the 3 positions and 8 gauges have been processed (Table 5). Since performing the characterization experiment across the entire continuous measurement range is not feasible, these 24 points will be used to interpolate the values throughout the full range, as illustrated in Figure 18.

**Table 5.** Set of accuracy and uncertainty values for each of the 24 data points.

| Height (mm) | Accuracy L (µm) | Accuracy C (µm) | Accuracy R (µm) | StdDev L (µm) | StdDev C (µm) | StdDev R (µm) |
|---|---|---|---|---|---|---|
| 5 | 0.432 | −0.156 | 1.813 | 0.73074 | 0.59858 | 0.60747 |
| 10 | −2.489 | 1.019 | 1.599 | 0.60796 | 0.59064 | 0.99641 |
| 20 | 0.337 | −5.789 | −3.166 | 0.60076 | 0.57965 | 0.56794 |
| 30 | 1.299 | 2.194 | −2.778 | 0.72873 | 0.61228 | 0.62389 |
| 40 | 2.822 | 2.303 | 2.027 | 0.73414 | 0.56818 | 0.61432 |
| 50 | 0.741 | −0.357 | −8.473 | 0.68355 | 0.58880 | 0.65949 |
| 60 | −0.775 | 0.792 | 3.876 | 0.65029 | 0.65646 | 0.94692 |
| 70 | −1.723 | −1.332 | 3.044 | 0.75904 | 0.59481 | 0.71523 |




(**a**) (**b**)

**Figure 18.** Results of expanded measurements to all the sensor ranges: (**a**) accuracy or bias error (**b**) standard deviation.

The different trend observed in the left region could not be unambiguously attributed to either the sensor itself or to a local geometrical deviation of the characterization setup. Therefore, no specific physical origin is assumed in the present study. From a metrological perspective, however, the measured deviation is explicitly incorporated into the sensor correction model.

### *3.3. Evaluation of the Integrated Digital Twin Through Real Scanning Scenarios.*

This section presents the final validation of the complete Digital Twin (DT) system, which integrates both the robotic platform and the optical measurement sensor. Unlike previous result sections, which examined the robot and sensor independently, the experiments described here assess the holistic behavior of the system following the hand–eye referencing process and full calibration. The evaluation is performed by comparing the DT-predicted measurement behavior against actual scanning outputs.

To this end, two experimental parts were employed:

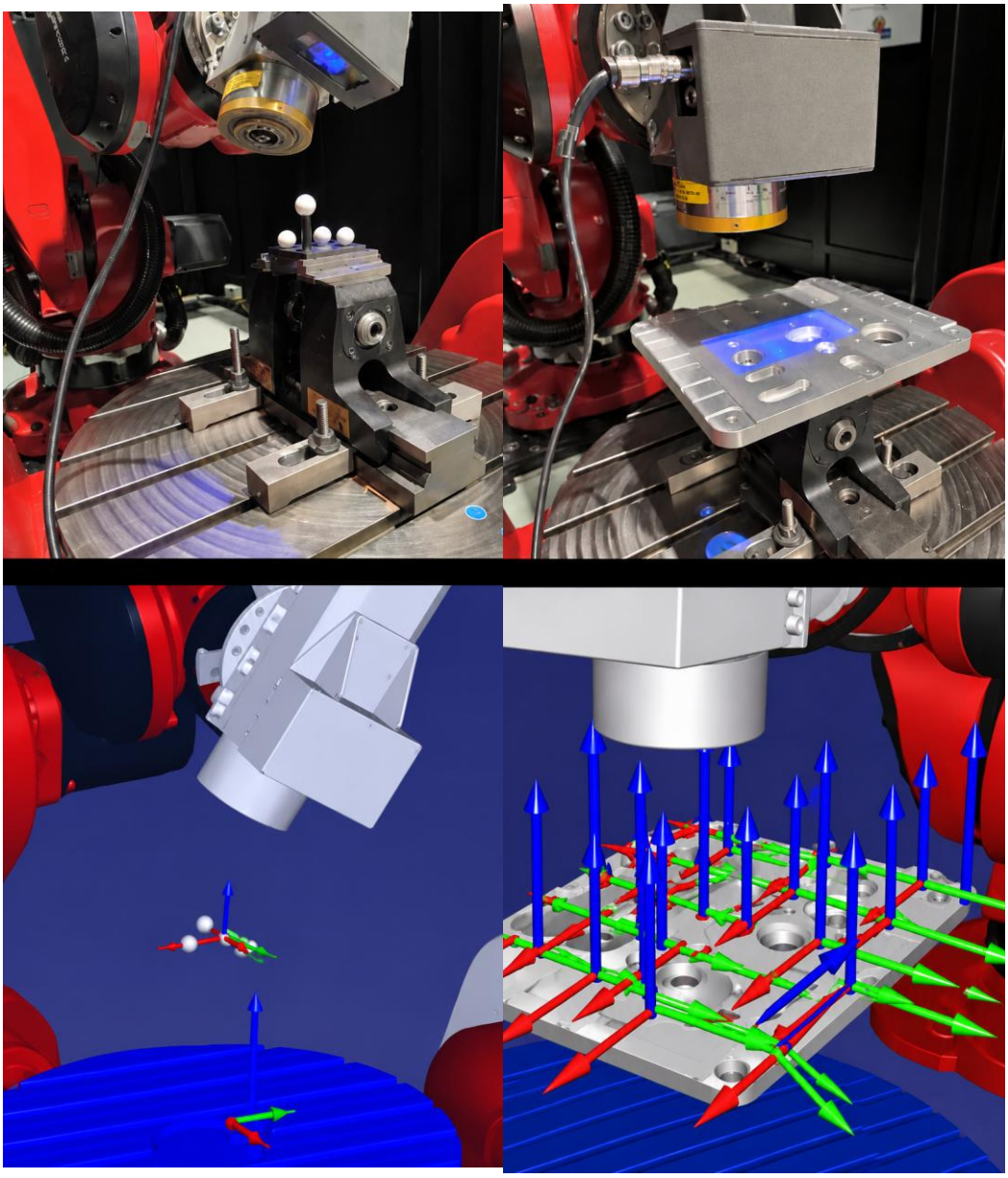
The first validation object was a four-sphere artifact previously characterized using a coordinate measuring machine (CMM). The calibrated sphere geometry provides a traceable reference and allows the integrated transformation and measurement chain to be evaluated using well-defined three-dimensional geometric features.

The second object was a geometrically complex validation part containing conventional geometric features and freeform regions. This part was used for dual-reference cross-validation. The freeform surfaces were compared against a dense reference surface acquired with a calibrated GOM ATOS III Triple Scan system, while selected dimensional

and geometrical characteristics were independently referenced by a ZEISS coordinate measuring machine (CMM). Task-specific uncertainty values for the CMM reference measurements were obtained from the corresponding virtual CMM (VCMM) workflow. This second case was selected to assess the DT using a geometry more representative of the intended inspection application and to complement global point-cloud comparison with feature-level metrological validation.

As shown in Figure 19, the scanning operations were performed using the integrated robotic and sensor system. The setup includes the following:

- The 4-ball calibrated artifact (Figure 19a), pre-measured with a coordinate measuring machine (CMM) to establish a high-precision reference;
- The freeform validation part (Figure 19b), used for two independent reference comparisons: a dense surface reference obtained with the calibrated Triple Scan system and feature-level reference measurements obtained with a ZEISS CMM/VCMM [19] workflow.



(**a**) (**b**)

**Figure 19.** Experimental validation setups: (**a**) four-sphere reference artifact; (**b**) freeform validation part scanned by the robotic inspection system.

The manufacturer-calibrated GOM ATOS III Triple Scan system was used to generate an independent dense reference surface for the freeform regions. The DT-based robotic point cloud was registered to this reference, and the resulting surface-deviation field was used for the surface-level cross-validation reported below.

Ten repeated acquisitions of the complex part were considered for the DT-based robotic system. For each evaluated characteristic, the mean DT result, $\bar{x}_{DT}$, and the experimental standard deviation of the repeated measurements, $s_{DT}$, were determined. The signed systematic difference with respect to the CMM reference value was calculated as

$$b = \bar{x}_{DT} - x_{CMM} \tag{9}$$

where $x_{CMM}$ is the corresponding CMM reference value.

Because the comparison is performed using the mean of n = 10 repeated DT measurements, the standard uncertainty associated with the mean DT result was estimated as

$$u_{\bar{x},DT} = \frac{s_{DT}}{\sqrt{n}} \tag{10}$$

The CMM report provides an expanded reference uncertainty, $U_{CMM}$, with a coverage factor K = 2. Therefore, the corresponding standard uncertainty of the CMM reference was obtained as

$$u_{CMM} = \frac{U_{CMM}}{2} \tag{11}$$

Assuming independence between the uncertainty associated with the mean DT result and the CMM reference uncertainty, the combined standard uncertainty associated with the cross-validation was evaluated as

$$u_{cv} = \sqrt{u_{\bar{x},DT}^2 + u_{CMM}^2} \tag{12}$$

The corresponding expanded uncertainty of the comparison was then calculated as

$$U_{cv} = k\, u_{cv} \tag{13}$$

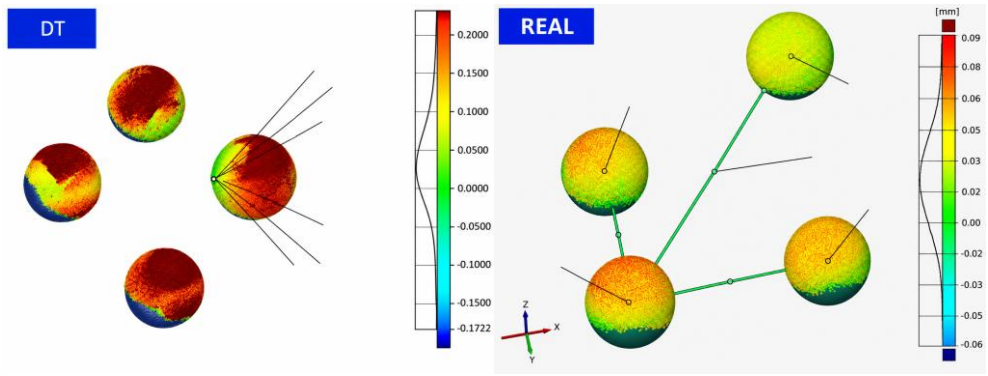
using k = 2 in the present study. The systematic difference, $b$, is reported separately from $U_{cv}$, so that any systematic disagreement between the DT-based measurement and the CMM reference is not incorporated into, and therefore hidden by, the random and reference-uncertainty contributions. The same complex-part dataset was also evaluated using GOM Inspect Professional 2017, providing an independent commercial-software route for the reported feature results. This comparison is used to support the independent evaluation of the measured geometrical characteristics and is not interpreted as a one-to-one benchmark of the uncertainty-propagation engine implemented in the DT.

In these experiments, the Digital Twin was employed to:

- Plan the scanning trajectories;
- Simulate point-wise uncertainty propagation using the GUM-compliant Monte Carlo Method (GUM-MCM), as described earlier in the Methods section;
- Compare the predicted (virtual) point cloud with the real-world scanned data.

#### 3.3.1. Results with the Calibrated Artifact

Figure 20 shows the DT- and physically measured deviations from the nominal geometry of the four-sphere artifact. The CMM characterization used as the traceable reference assigns an expanded uncertainty of 0.002 mm (k = 2) to the reported sphere diameters and sphere-center coordinates. The DT simulations, executed with Monte Carlo uncertainty propagation, show the residual variation in the integrated robot–sensor chain after calibration, with the comparison summarized below.




(**a**) (**b**)

**Figure 20.** Four-sphere validation artifact: (**a**) point-wise deviations predicted by the Digital Twin using Monte Carlo uncertainty propagation; (**b**) corresponding deviations obtained from the physical robot–sensor measurement.

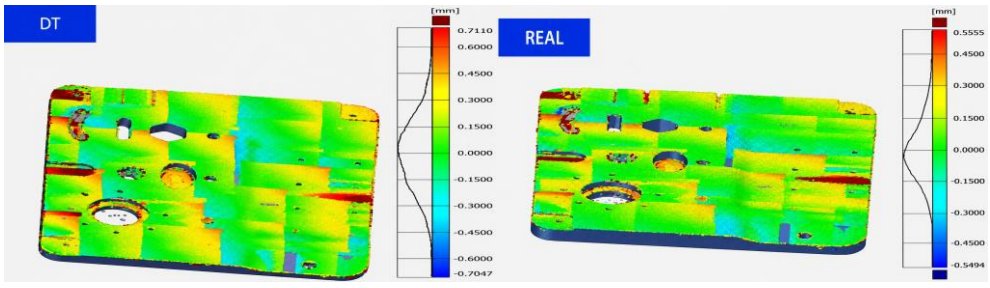
These results (Table 6) demonstrate DT's ability to estimate point-wise uncertainty with a reasonable level of accuracy. Although the simulated cloud shows slightly higher residual deviations, it maintains credible consistency with the ground-truth CMM data. This outcome validates the effectiveness of the Monte Carlo approach to propagate uncertainties from joint, sensor, and referencing parameters into the cloud level.

**Table 6.** Comparison of mean error and standard deviation for calibrated 4-sphere artifact–digital twin vs. real measurement.

| Metric | Digital Twin | Real |
|---|---|---|
| Mean error (μm) | 40 | 10 |
| Standard deviation (μm) | 30 | 20 |

3.3.2. Results with the Geometric and Freeform Validation Part

Figure 21 presents the results for the second part, featuring more complex geometries. Table 7 shows that the global mean deviation is approximately 1 μm for both datasets, whereas the DT-based robotic result exhibits a broader distribution (standard deviation of 125 μm) than the Triple Scan reference (91 μm). The close global mean indicates similar overall alignment, while the difference in dispersion motivates the feature-level CMM analysis presented in the following subsection.




(**a**) (**b**)

**Figure 21.** Geometric/freeform validation part: (**a**) Digital-Twin-predicted point-cloud deviations and uncertainty distribution; (**b**) corresponding experimental robotic measurement used for comparison.

**Table 7.** Comparison of mean error and standard deviation for the geometric/freeform validation part: Digital Twin versus physical measurement.

| Metric | DT-Based System | Ref. |
|---|---|---|
| Mean deviation (µm) | 1 | 1 |
| Standard deviation (µm) | 125 | 91 |

The surface-level comparison and the feature-level dimensional comparison describe different aspects of metrological agreement. A global point-cloud mean can remain close to zero because local positive and negative deviations partially compensate, whereas fitted geometric characteristics are more sensitive to local shape, alignment, and transformation errors. The CMM-based cross-validation below is therefore used to assess the DT at measurand level rather than relying only on global cloud statistics.

#### 3.3.3. Feature-Level Cross-Validation Against CMM/VCMM

The additional CMM cross-validation covers 19 feature groups representing 67 evaluated characteristics, including flatness, diameter, individual positioning, surface-profile error, and composed positioning. Table 8 summarizes the range of absolute DT-CMM differences, the short-term repeatability observed over the repeated DT acquisitions, the task-specific expanded CMM/VCMM reference uncertainty, and the resulting comparison uncertainty $U_{cv}$. The CMM/VCMM uncertainties are markedly smaller than the largest DT-CMM differences, so the larger discrepancies observed for some measurands cannot be explained by reference uncertainty alone. For example, the reference cylinder diameter was 38.1195 mm compared with 38.1090 mm from the DT-based system ($|\Delta|$ = 10.5 µm), whereas one composed-positioning result differed by only 0.2 µm. In contrast, the large-surface profile result showed a 126.5 µm difference, illustrating that local geometry-dependent effects are more discriminating than the global surface mean reported in Table 7.

The Triple Scan route provides a dense surface reference for the freeform geometry, whereas the CMM/VCMM route provides traceable feature values together with task-specific uncertainty. Their combined use avoids relying on a single reference technology and provides complementary surface-level and measurand-level evidence for the integrated DT.

**Table 8.** Feature-level CMM/VCMM cross-validation of the complex part. Absolute DT-CMM differences and short-term DT repeatability are reported together with the task-specific CMM/VCMM expanded reference uncertainty (k = 2).

| Property | Groups/ Features | \|DT–CMM\| (µm) | $s_{DT}$ (µm) | $u_{\bar{x},DT}$ (µm) | $U_{CMM}$ (k = 2) (µm) | $U_{cv}$ (k = 2) (µm) |
|---|---|---|---|---|---|---|
| Flatness | 3/3 | 44.6–176.2 | 8–9 | 2.5–2.8 | 0.4–5.8 | 5.1–8.1 |
| Diameter | 9/41 | 3.5–170.3 | 2–10 | 0.6–3.2 | 0.4–2.3 | 1.3–6.7 |
| Positioning | 2/2 | 17.4–42.6 | 3–8 | 0.9–2.5 | 3.2–4.5 | 3.7–6.8 |
| Profile error | 2/2 | 44.1–126.5 | 2–17 | 0.6–5.4 | 5.5–6.6 | 5.6–12.6 |
| Composed positioning | 3/19 | 0.2–41.1 | 7–9 | 2.2–2.8 | 1.7–4.3 | 4.7–7.1 |

## 4. Discussion

The extended validation demonstrates that surface-level and feature-level comparisons provide complementary information about the metrological behavior of the integrated robot–sensor system. The Triple Scan comparison gives similar global mean deviations for the DT-based and reference surfaces, while the broader DT distribution reflects the propagated variability of the calibrated measurement chain. In contrast, the

CMM/VCMM cross-validation across 67 characteristics reveals measurand-dependent systematic differences ranging from 0.2 µm to 176.2 µm. A near-zero global point-cloud mean should therefore not be interpreted as equivalent to micrometer-level agreement for every fitted geometric characteristic.

The feature-level results also help separate reference quality from system behavior. Short-term DT repeatability remains between 2 µm and 17 µm across the evaluated categories, while the CMM/VCMM expanded reference uncertainties range from 0.4 µm to 6.6 µm. The largest discrepancies, particularly for flatness and surface-profile quantities, are therefore dominated by residual systematic or geometry-dependent effects rather than by the CMM reference uncertainty. Conversely, the close agreement obtained for selected diameter and composed-positioning characteristics shows that the integrated DT can reproduce some measurands within a few micrometers under the investigated conditions. This heterogeneity reinforces the need for task-specific uncertainty evaluation instead of a single global accuracy figure.

The additional evaluation in GOM Inspect Professional 2017 provides an independent commercial-software route for the complex-part feature results, while the ZEISS CMM/VCMM workflow supplies traceable reference values and task-specific uncertainty information. This should not be interpreted as a direct one-to-one benchmark of uncertainty engines: the commercial tools evaluate optical/CMM measurement results, whereas the proposed DT explicitly propagates uncertainty through the calibrated robot kinematics, optical sensor, and sensor-to-robot referencing chain. The comparison is therefore made at the level of reported measurement results and reference uncertainty.

Thermal and environmental effects remain outside the experimentally validated scope of the present model. Temperature was not recorded as an independent input during the campaign, and no thermo-geometric correction model was identified. Accordingly, the reported DT state and uncertainty results are valid only for the environmental conditions under which calibration, referencing, and validation were performed. Deployment under variable shop-floor conditions would require explicit environmental sensing and validation of temperature-dependent robot, sensor, and referencing contributions.

Similarly, the repeated measurements available in this study characterize short-term repeatability rather than long-term stability. No extended drift experiment or repeated independent calibration campaign was available to establish temporal drift rates or a validated recalibration interval. Although the P2V/V2P architecture supports periodic recalibration and state updates, this capability should be regarded as an architectural provision rather than experimental evidence of long-term stability. The present work therefore establishes the metrological DT framework and its short-term experimental cross-validation, while full industrial qualification requires dedicated thermal and temporal stability studies.

Within these limits, the proposed architecture remains transferable at the methodological level because robot calibration, sensor characterization, referencing, reference data, and uncertainty information are represented as separate elements of the DT. Application to another robot–sensor configuration would require system-specific calibration and validation data while preserving the same traceability and uncertainty-propagation structure.

## 5. Conclusions

This work presents a traceable metrological Digital Twin for robot-based 3D inspection that integrates robot calibration, optical-sensor characterization, sensor-to-robot reference, machine-readable metrological information, and Monte Carlo uncertainty propagation within a common measurement framework.

The integrated system was cross-validated using a CMM-characterized four-sphere artifact and a geometrically complex part. For the latter, two complementary reference routes were used: a calibrated Triple Scan system for dense surface comparison and a ZEISS CMM/VCMM workflow for feature-level validation. The additional CMM analysis covers 19 feature groups representing 67 characteristics and shows that measurement agreement is measurand-dependent. While selected characteristics agree within a few micrometers, larger differences are observed for some flatness and profile quantities, demonstrating the value of feature-level cross-validation in addition to global point-cloud statistics.

The present results characterize the calibrated system under the environmental conditions and time scale of the experimental campaign. Thermal effects are not explicitly modeled, and long-term drift has not been experimentally quantified; therefore, the work should be interpreted as a metrological framework with short-term experimental validation rather than a complete industrial qualification. Future work should incorporate environmental sensing, validated thermo-geometric models, and long-duration reference measurements to establish robust recalibration intervals for variable shop-floor operation.

**Author Contributions:** Conceptualization, B.A.C., A.G.B. and P.P.; methodology, B.A.C., A.G.B., P.P. and J.F.; software, B.A.C., A.G.B. and J.F.; validation, B.A.C., A.G.B. and J.F.; formal analysis, B.A.C., A.G.B., P.P. and J.F.; investigation, B.A.C. and P.P.; resources, B.A.C. and P.P.; data curation, B.A.C. and A.G.B.; writing—original draft preparation, B.A.C., A.G.B., P.P. and J.F.; writing—review and editing, B.A.C., A.G.B., P.P., J.F. and N.O.R.; visualization, B.A.C., A.G.B. and J.F.; supervision, B.A.C., P.P., J.F., L.T. and B.H.; project administration, B.A.C., P.P., J.F., L.T. and B.H. All authors have read and agreed to the published version of the manuscript.

**Funding:** The project (22DIT01 ViDiT) has received funding from the European Partnership on Metrology, co-financed by the European Union's Horizon Europe Research and Innovation Programme and by the Participating States. Funder name: European Partnership on Metrology. Funder ID: 10.13039/100019599. Grant number: 22DIT01 ViDiT. METROtek (Grant No: KK-2024/00080), funded by the Department of Industry, Energy Transition and Sustainability of the Basque Government through the Elkartek Program for Collaborative Research in Strategic Areas. The project (23IND08 DI-Vision) has received funding from the European Partnership on Metrology, co-financed by the European Union's Horizon Europe Research and Innovation Programme and by the Participating States. Funder name: European Partnership on Metrology. Funder ID: 10.13039/100019599. Grant number: 23IND08 DI-Vision.

**Institutional Review Board Statement:** Not applicable.

**Informed Consent Statement:** Not applicable.

**Data Availability Statement:** The raw data supporting the conclusions of this article will be made available by the authors on request.

**Conflicts of Interest:** The authors declare no conflicts of interest.

## References

1. Jones, D.; Snider, C.; Nassehi, A.; Yon, J.; Hicks, B. Characterising the Digital Twin: A Systematic Literature Review. *CIRP J. Manuf. Sci. Technol.* **2020**, *29*, 36–52. https://doi.org/10.1016/J.CIRPJ.2020.02.002.
2. *ISO 23247-1:2021*; Automation Systems and Integration—Digital Twin Framework for Manufacturing—Part 1: Overview and General Principles. International Organization for Standardization (ISO): Geneva, Switzerland, 2021 https://www.iso.org/es/contents/data/standard/07/50/75066.html.
3. Maculotti, G.; Marschall, M.; Kok, G.; Chekh, B.A.; van Dijk, M.; Flores, J.; Genta, G.; Puerto, P.; Galetto, M.; Schmelter, S. A Shared Metrological Framework for Trustworthy Virtual Experiments and Digital Twins. *Metrology* **2024**, *4*, 337–363. https://doi.org/10.3390/metrology4030021.

4. Catalucci, S.; Thompson, A.; Piano, S.; Branson, D.T.; Leach, R. Optical Metrology for Digital Manufacturing: A Review. *Int. J. Adv. Manuf. Technol.* **2022**, *120*, 4271–4290. https://doi.org/10.1007/S00170-022-09084-5.
5. Lin, T.Y.; Jia, Z.; Yang, C.; Xiao, Y.; Lan, S.; Shi, G.; Zeng, B.; Li, H. Evolutionary Digital Twin: A New Approach for Intelligent Industrial Product Development. *Adv. Eng. Inform.* **2021**, *47*, 101209. https://doi.org/10.1016/J.AEI.2020.101209.
6. Havard, V.; Jeanne, B.; Lacomblez, M.; Baudry, D. Digital Twin and Virtual Reality: A Co-Simulation Environment for Design and Assessment of Industrial Workstations. *Prod. Manuf. Res.* **2019**, *7*, 472–489. https://doi.org/10.1080/21693277.2019.1660283.
7. Kousi, N.; Gkournelos, C.; Aivaliotis, S.; Giannoulis, C.; Michalos, G.; Makris, S. Digital Twin for Adaptation of Robots' Behavior in Flexible Robotic Assembly Lines. *Procedia Manuf.* **2019**, *28*, 121–126. https://doi.org/10.1016/J.PROMFG.2018.12.020.
8. Cai, Y.; Wang, Y.; Burnett, M. Using Augmented Reality to Build Digital Twin for Reconfigurable Additive Manufacturing System. *J. Manuf. Syst.* **2020**, *56*, 598–604. https://doi.org/10.1016/J.JMSY.2020.04.005.
9. Matulis, M.; Harvey, C. A Robot Arm Digital Twin Utilising Reinforcement Learning. *Comput. Graph.* **2021**, *95*, 106–114. https://doi.org/10.1016/J.CAG.2021.01.011.
10. Meana, V.; Zapico, P.; Cuesta, E.; Giganto, S.; Martinez-Pellitero, S. Laser Triangulation Sensors Performance in Scanning Different Materials and Finishes. *Sensors* **2024**, *24*, 2410. https://doi.org/10.3390/S24082410.
11. Mohammadikaji, M.; Bergmann, S.; Irgenfried, S.; Beyerer, J.; Dachsbacher, C.; Worn, H. A Framework for Uncertainty Propagation in 3D Shape Measurement Using Laser Triangulation. In *2016 IEEE International Instrumentation and Measurement Technology Conference Proceedings*; IEEE: New York, NY, USA, 2016. https://doi.org/10.1109/I2MTC.2016.7520324.
12. Wübbeler, G.; Marschall, M.; Kniel, K.; Heißelmann, D.; Härtig, F.; Elster, C. GUM-Compliant Uncertainty Evaluation Using Virtual Experiments. *Metrology* **2022**, *2*, 114–127. https://doi.org/10.3390/METROLOGY2010008.
13. Zhao, Y.; Zhou, Y.; Gu, R.; Wang, Z.; Cheng, Y. Uncertainty Analysis of Dimension Calibration for Line Laser Scanning Measurement System. In Proceedings of the 2021 IEEE 15th International Conference on Electronic Measurement & Instruments (ICEMI), Nanjing, China, 29–31 October 2021; pp. 370–376. https://doi.org/10.1109/ICEMI52946.2021.9679495.
14. Ostrowska, K.; Owczarek, D.; Gąska, A.; Krawczyk, M.; Kupiec, R.; Sładek, J. Assumptions of the Digital Twin in Coordinate Metrology. *Meas. Sens.* **2025**, *38*, 101667. https://doi.org/10.1016/J.MEASEN.2024.101667.
15. Vlaeyen, M.; Haitjema, H.; Dewulf, W. Digital Twin of an Optical Measurement System. *Sensors* **2021**, *21*, 6638. https://doi.org/10.3390/s21196638.
16. Sepahi-Boroujeni, S., Khameneifar, F. Digital twin-enabled error and uncertainty mapping for 3D scanning. *Precis. Eng.* **2024**, *88*, 527–539. https://doi.org/10.1016/J.PRECISIONENG.2024.03.007
17. Nubiola, A.; Bonev, I.A. Absolute Calibration of an ABB IRB 1600 Robot Using a Laser Tracker. *Robot. Comput. Integr. Manuf.* **2013**, *29*, 236–245. https://doi.org/10.1016/j.rcim.2012.06.004.
18. Garmendia, I.; Flores, J.; Madarieta, M.; Lamikiz, A.; Uriarte, L.G.; Soriana, C. Geometrical Control of DED Processes Based on 3D Scanning Applied to the Manufacture of Complex Parts. *Procedia CIRP* **2020**, *94*, 425–429. 10.1016/j.procir.2020.09.158.
19. Trapet, E.; Franke, M.; Härtig, F.; Schwenke, H.; Wäldele, F.; Cox, M.; Forbes, A.; Delbressine, F.; Schellekens, P.; Trenk, M.; et al. *Traceability of Coordinate Measurements According to the Method of the Virtual Measuring Machine: Part 2 of the Final Report Project MAT1-CT94-0076*; Wirtschaftsverlag NW: Bremerhaven, Germany, 1999; 147p.


**Disclaimer/Publisher's Note:** The statements, opinions and data contained in all publications are solely those of the individual author(s) and contributor(s) and not of MDPI and/or the editor(s). MDPI and/or the editor(s) disclaim responsibility for any injury to people or property resulting from any ideas, methods, instructions or products referred to in the content.